Check for updates

The Meteoritical Society

Meteoritics & Planetary Science 57, Nr 6, 1247–1266 (2022)
doi: 10.1111/maps.13818

Artificial weathering of an ordinary chondrite: Recommendations for the curation of Antarctic meteorites

Matthias van GINNEKEN[1]*, Vinciane DEBAILLE[2], Sophie DECRÉE[3], Steven GODERIS[4], Alan B. WOODLAND[5], Penelope WOZNIAKIEWICZ[1], Marleen De CEUKELAIRE[3], Thierry LEDUC[3], and Philippe CLAEYS[4]

[1]Centre for Astrophysics and Planetary Science, School of Physical Sciences, Ingram Building, University of Kent, Canterbury CT2 7NH, UK
[2]Laboratoire G-Time, Université Libre de Bruxelles, Brussels BE1050, Belgium
[3]Geological Survey of Belgium, Royal Belgian Institute of Natural Sciences, rue Vautier 29, Brussels BE1000, Belgium
[4]Analytical, Environmental, and Geochemistry, Vrije Universiteit Brussel, Pleinlaan 2, Brussels BE1050, Belgium
[5]Institut für Geowissenschaften, Goethe-Universität Frankfurt, Altenhöferallee 1, Frankfurt am Main D-60438, Germany
*Corresponding author. E-mail: m.van-ginneken@kent.ac.uk

(Received 09 November 2021; revision accepted 28 March 2022)

Abstract–Meteorites are prone to errestrial weathering not only after their fall on the Earth's surface but also during storage in museum collections. To study the susceptibility of this material to weathering, weathering experiments were carried out on polished sections of the H5 chondrite Asuka 10177. The experiments consisted of four 100-days cycles during which temperature and humidity varied on a twelve hours basis. The first alteration cycle consisted of changing the temperature from 15 to 25 °C; the second cycle consisted of modifying both humidity and temperature from 35 to 45% and 15 to 25 °C, respectively; the third cycle consisted of varying the humidity level from 40 to 60%; and the fourth cycle maintained a fixed high humidity of 80%. Weathering products resulting from the experiments were identified and characterized using scanning electron microscopy–energy dispersive spectroscopy and Raman spectroscopy. Such products were not observed at the microscopic scale after the first cycle of alteration. Conversely, products typical of the corrosion of meteoritic FeNi metal were observed during scanning electron microscope surveys after all subsequent cycles. Important increases in the distribution of weathering products on the samples were observed after cycles 2 and 4 but not after cycle 3, suggesting that the combination of temperature and humidity fluctuations or high humidity (>60%) alone is most detrimental to chondritic samples. Chemistry of the weathering products revealed a high degree of FeNi metal corrosion with a limited contribution of troilite corrosion. No clear evidence of mafic silicate alteration was observed after all cycles, suggesting that postretrieval alteration remains limited to FeNi metal and to a lesser extent to troilite.

INTRODUCTION

Meteorites have been a subject of scientific scrutiny for centuries, even before the publication of Chladni's book in 1794 arguing that these unusual rocks came from space (Marvin, 2006; McCall et al., 2006). The fall of the Wold Cottage and L'Aigle meteorites in 1795 and 1803, respectively, was paramount to convince the scientific community that meteorites were indeed extraterrestrial in origin (Gounelle, 2006). Significant efforts around the world have focused on the acquisition of samples to establish meteorite collections ever since. The oldest and one of the biggest repositories of meteorites is held at the Museum of Natural History in Vienna, Austria, which was founded in the mid-18th century (Brandstätter, 2006). Following this trend, museums and research institutes all over the world started establishing their own meteorite

© 2022 The Authors. *Meteoritics & Planetary Science* published by Wiley Periodicals LLC on behalf of The Meteoritical Society.
This is an open access article under the terms of the Creative Commons Attribution License, which permits use, distribution and reproduction in any medium, provided the original work is properly cited.

collections (Caillet Komorowski, 2006; Ebel, 2006; Russell & Grady, 2006). However, even though this field attracted a lot of attention, technical limitations prevented detailed analyses of samples up until a considerable technological leap forward in the mid-20th century, when the invention of the scanning electron microscopy and electron probe microanalyses allowed an unprecedented level of accuracy and precision for chemical and petrological analyses. Shortly thereafter, meteoriticists expanded the classification scheme that is still used today (Brearley & Jones, 1998; Krot et al., 2007; Mittlefehldt et al., 1998; Van Schmus & Wood, 1967; Weisberg et al., 2006). Another limitation to the study of meteorites was the limited number of samples available to the scientific community, which in the early 1970s was around 2000. The discovery of nine meteorites in Antarctica during the 1969 Japanese Antarctic Research Expedition started the most crucial chapter in the history of modern meteoritics: the systematic search for meteorites in Antarctica (Kojima, 2006). Within two decades, the number of samples available to the scientific community increased by an order of magnitude. The discovery of numerous samples in hot deserts, mainly Northwest Africa, in the late 1980s, further increased the size of collections worldwide (Bevan, 2006). More recently, thousands of meteorites have been found in other hot deserts such as the Oman, Atacama, and Libyan Deserts (Al-Kathiri et al., 2005; Drouard et al., 2019; Schlüter et al., 2002). Since 2009, Belgium has been a key player in this field, with the discovery of more than 1200 meteorites in the blue ice field surrounding the Sør Rondane Mountains, Queen Maud Land, Antarctica (De Ceukelaire et al., 2013; Kaiden et al., 2011; Zekollari et al., 2019), near the Princess Elisabeth Antarctica research station (Fig. A1 in supporting information). Belgian expeditions for the search of meteorites were carried out within the framework of a collaboration between the Université Libre de Bruxelles (ULB), Vrije Universiteit Brussel (VUB), and the Japanese National Institute of Polar Research (NIPR). Collected samples are equally divided between the NIPR and the Belgian institutions, which then store them at the Royal Belgian Institute of Natural Sciences (RBINS).

Meteorites are rare and precious samples by essence; their preservation from detrimental effects from the terrestrial environment is essential. This is particularly the case now that sample return missions, such as Hayabusa and Hayabusa 2, allow comparisons between meteorites and pristine asteroid samples that are curated to minimize interaction with the terrestrial environment (Yada et al., 2014). Conversely, all meteorites interact with the terrestrial environment to a certain extent. The meteorites for which the fall was observed and that were collected shortly afterward show the lowest degree of interaction with the terrestrial environment, even though some minerals such as oldhamite break down in a matter of hours (Fogel, 1997; Okada et al., 1981). Still these falls are considered the most pristine samples available in collections. The interaction of a meteorite with the Earth's environment results in terrestrial weathering that varies in extent depending on factors such as interaction with a fluid and the terrestrial age of a meteorite (i.e., time spent on the surface of the Earth; Bland et al., 2006). Indeed, the overwhelming majority of meteorites were collected on the Earth's surface a long time after their fall (i.e., the so-called "finds"), sometimes hundreds of thousands and even millions of years in the case of Antarctica (Jull, 2001; Nishiizumi et al., 1989; Welten et al., 2008). The most visible weathering products on meteorites are evaporites and rust (mainly Fe oxyhydroxides), which result from the precipitation of salts due to water evaporation and corrosion of metal within the rock, respectively (Benoit & Sears, 1999; Bland et al., 2006; Gooding, 1982, 1986; Jull et al., 1988; Lee & Bland, 2004; Losiak & Velbel, 2011; Velbel, 1988, 2014; Velbel & Gooding, 1990). Therefore, effects of terrestrial weathering are visible in most Antarctic meteorites, albeit to a much lower extent than in meteorites recovered under a more humid and/or hot climate (Bland et al., 2006; Maeda et al., 2021; Pourkhorsandi et al., 2021). Even though terrestrial weathering is unavoidable, it is nonetheless necessary to preserve collected meteorite samples in an environment that will slow or, ideally, stop its progression. To mitigate these effects, museums and research institutes worldwide have curation facilities entirely dedicated to meteorites (e.g., Righter et al., 2014). Such facilities vary significantly from one institute to the other, mainly depending on the nature of the meteoritic samples (e.g., unique volatile-rich falls such as the Tagish Lake meteorite require specifically designed curation facilities; McCubbin et al., 2019). However, the curation of large meteorite collections requires significant financial and human resources. Therefore, it is essential to understand how environmental factors (i.e., mainly temperature and humidity) in a curation facility affect meteorites to make them as effective at preserving them as possible. The main aim of this project was to test how meteorites react to changes in temperature and relative humidity. To study the effect of the variations of these two parameters, an H chondrite was artificially altered in a controlled climatic chamber following a set of weathering cycles. We observe a clear influence of variations in humidity on the formation of weathering products, with a lesser influence of variations in temperature. This work offers perspectives for the preservation and curation of meteorite samples stored in collections.

19455100, 2022, 6, Downloaded from https://onlinelibrary.wiley.com/doi/10.1111/maps.13818 by EVIDENCE AID - BELGIUM, Wiley Online Library on [07/06/2023]. See the Terms and Conditions (https://onlinelibrary.wiley.com/terms-and-conditions) on Wiley Online Library for rules of use; OA articles are governed by the applicable Creative Commons License

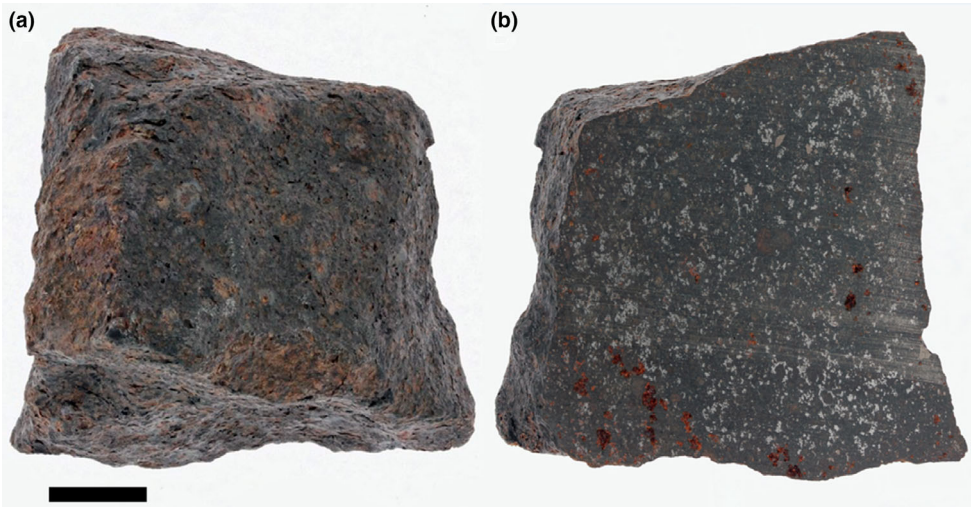

Fig. 1. Photographs of the A10177 sample held at the RBINS. a) Photograph of the exterior of A10177. The black area corresponds to the fusion crust that has not flaked off. Brownish red patches correspond to "metallic rust," which is a common terrestrial alteration product of FeNi metal in Antarctic meteorites (Bland et al., 2006; Gooding, 1986). b) Photograph of a section showing the interior of A10177. The brownish areas near the edge of the sample correspond to weathered FeNi metal grains to limonite. In the most severe cases, the metal dissolved entirely, leaving cavities partially filled with weathering products. Light gray patches visible in the interior of the sample correspond to pristine FeNi metal grains, showing that the meteorite is only superficially weathered. (Color figure can be viewed at wileyonlinelibrary.com.)

SAMPLES AND METHODS

Samples

The weathering experiments were carried out on the H5 ordinary chondrite Asuka 10177 (hereafter A10177), which was selected from the RBINS meteorite collection. The H chondrites are mainly composed of silicate minerals such as olivine and low-Ca pyroxene, with up to approximately 20 wt% FeNi metal and 5 wt% troilite (Brearley & Jones, 1998; Gattacceca et al., 2014). This chondrite was recovered during the 2010–2011 Belgian Antarctic Research Expedition (BELARE)/Japanese Antarctic Research Expedition (JARE) joint expedition within the Nansen ice field (approximately 72.7°S, 24.2°E), south of the Sør Rondane Mountains chain, Dronning Maud Land, Antarctica (Fig. A1). Upon recovery, the mass of A10177 was 233.82 g. The weathering grade is B/C (Ruzicka et al., 2017). This weathering scale was created to describe the occurrences of weathering products on hand specimens, and not polished sections. A weathering grade of B/C means that all metal grains observed with the naked eye on the surface of the meteorite were altered to limonite (Fig. 1a). It is noteworthy that this alteration occurred prior to collection during the presence of the meteorite in the Antarctic environment. Although the terrestrial age of this meteorite is unknown, a recent study shows that the terrestrial age of meteorites recovered from the Nansen ice field ranges from a few thousand years up to several tens of thousands of years (Zekollari et al., 2019). Thus, it is likely that A10177 fell several thousand years before being recovered.

Following its recovery in Antarctica, A10177 was cut in half and split between the RBINS and the NIPR in Tachikawa, Japan. Approximately 105 g is currently being held in the RBINS collection. The sectioning of A10177 revealed a largely fresh interior devoid of visible effects of weathering and exhibiting large patches of FeNi metal more than 1 cm in size (Fig. 1b).

This meteorite was chosen for the weathering experiments based on the following criteria:

1. Large sample size, allowing for the preparation of centimeter-scale subsamples.
2. H chondrites represent approximately 46% of ordinary chondrites, which in turn account for 80% of all chondrites (Brearley & Jones, 1998). Rare and precious samples (i.e., achondrites or carbonaceous chondrites) must be avoided in this type of study as the experiments effectively damage the samples.
3. The weathering scale, which is based on petroscopic observation of polished sections as opposed to hand specimens for the aforementioned weathering grade, is W1, meaning "Minor oxide rims around metal and troilite; minor oxide veins" (Fig. 2) (Wlotzka, 1993). A sample as pristine as reasonably possible is necessary for these experiments.

Five fragments of A10177 of approximately 1 × 0.5 cm in size were prepared at the RBINS and

19455100, 2022, 6, Downloaded from https://onlinelibrary.wiley.com/doi/10.1111/maps.13818 by EVIDENCE AID - BELGIUM, Wiley Online Library on [07/06/2023]. See the Terms and Conditions (https://onlinelibrary.wiley.com/terms-and-conditions) on Wiley Online Library for rules of use; OA articles are governed by the applicable Creative Commons License

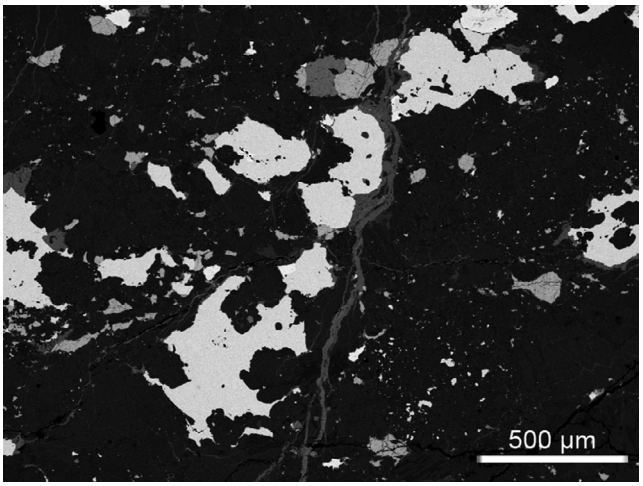

Fig. 2. Scanning electron backscattered image of a representative area of A10177, showing the extent of terrestrial weathering suffered by the meteorite in the Antarctic environment. White areas represent elements with a high Z-contrast, such as FeNi metal; dark gray areas represent elements with a low Z-contrast, such as silicate phases; light gray areas represent weathering product ferrihydrite rims around FeNi metal grains and veins filling preexisting cracks.

were subsequently embedded in epoxy resin and polished. The fragments were labeled MET-1 to 5.

Experimental Methods

The weathering experiments were carried out using a Weiss Technik WKL 34/40 climatic chamber at the Laboratoire G-Time of the ULB. This instrument allows experiments over a wide range of temperatures and humidity, that is, −72 to +100 °C and 20–90%, respectively. The control of the relative humidity consisted of the injection (i.e., increasing humidity) or purging (i.e., decreasing humidity) of demineralized water. On this instrument, precise temperature and humidity cycles can be programmed to last indefinitely or over a fixed period. Over the course of the project, four 100-day alteration cycles were undertaken. Each cycle consisted of variations in temperature and/or humidity on a 12 h basis (Fig. 3). A10177 fragments were exposed in the climatic chamber to the various weathering cycles. Subsample MET-1 was kept in storage as a witness sample.

The first alteration cycle consisted of varying the temperature only in the climatic chamber. The temperature varied from 15 to 25 °C every 12 h, with a fixed humidity of 30%. After this first cycle, artificially altered sample MET-2 was studied using a scanning electron microscope (SEM) at VUB. Subsequently, the surface of MET-2 was drilled using a 300 µm wide tip drill at the VUB to extract potential weathering products for subsequent Mössbauer spectroscopy analyses.

The second cycle consisted of changing both the humidity and temperature every 12 h, from 35 to 45% and 15 to 25 °C, respectively. Samples MET-2 and MET-3 were then examined using an FEI Quanta 300 SEM at the RBINS. The chemical composition of weathering products was determined used an EDAX energy-dispersive spectroscopy (EDS) detector. All observations were carried out at 15 kV to avoid deteriorating the weathering products. Additional EDS analyses and element mapping were carried using a Hitachi S4700 Field Emission Gun SEM equipped with a Bruker X-Flash Quad EDX detector at the School of Physical Science, University of Kent, United Kingdom. This annular EDS detector presents the advantage of allowing precise EDS analyses and chemical mapping of rough samples.

Approximately 1 mg of the MET-2 powder was sent to the Institut für Geowissenschaften Fachbereich of the Goethe Universität, Frankfurt am Main, Germany, to determine the relative abundances of Fe^0, Fe^{2+}, and Fe^{3+} in the altered area using Mössbauer spectroscopy, which should reflect the amount of Fe-oxyhydroxide in the sample. Mössbauer analyses were carried out at room temperature using a standard Mössbauer spectrometer. Spectra were obtained in constant acceleration mode with a velocity ramp of approximately ± 12 mm s^{-1} and were calibrated with respect to α-Fe metal. Approximately 1 mg of drilled powder from sample MET-1 (i.e., witness sample) was also included in the Mössbauer analyses for comparison. The third cycle on sample MET-4 consisted in changing humidity only from 40 to 60% every 12 h. Finally, a fourth cycle on MET-5 consisted of maintaining a high humidity of 80% continuously. For both MET-4 and MET-5 experiments (cycles 3 and 4), the temperature was fixed at 20 °C. Micro-Raman spectroscopy at the RBINS was used to characterize the weathering phases in MET-3, MET-4, and MET-5. The instrument used is a SENTERRA dispersive Raman microscope (BRUKER) at the RBINS, equipped with a thermoelectrically cooled CCD (ANDOR DU420-OE). The spectral resolution applied is ~9 cm^{-1} in the 200–1200 cm^{-1} range (50 × 1000 µm slit) and a continuous automatic calibration (0.1 cm^{-1} accuracy) with a solid-state laser corresponding to red light (784 nm) at 2 mW for excitation. Raman spectra were processed using the software Spectragryph by Friedrich Menges. Reference spectra from the RRUFF online database were used to identify mineral species (Lafuente et al., 2016).

RESULTS

After the first cycle, which consisted of changing the temperature only, MET-2 did not exhibit structural or petrographic changes commonly observed in weathered

19455100, 2022, 6, Downloaded from https://onlinelibrary.wiley.com/doi/10.1111/maps.13818 by EVIDENCE AID - BELGIUM, Wiley Online Library on [07/06/2023]. See the Terms and Conditions (https://onlinelibrary.wiley.com/terms-and-conditions) on Wiley Online Library for rules of use; OA articles are governed by the applicable Creative Commons License

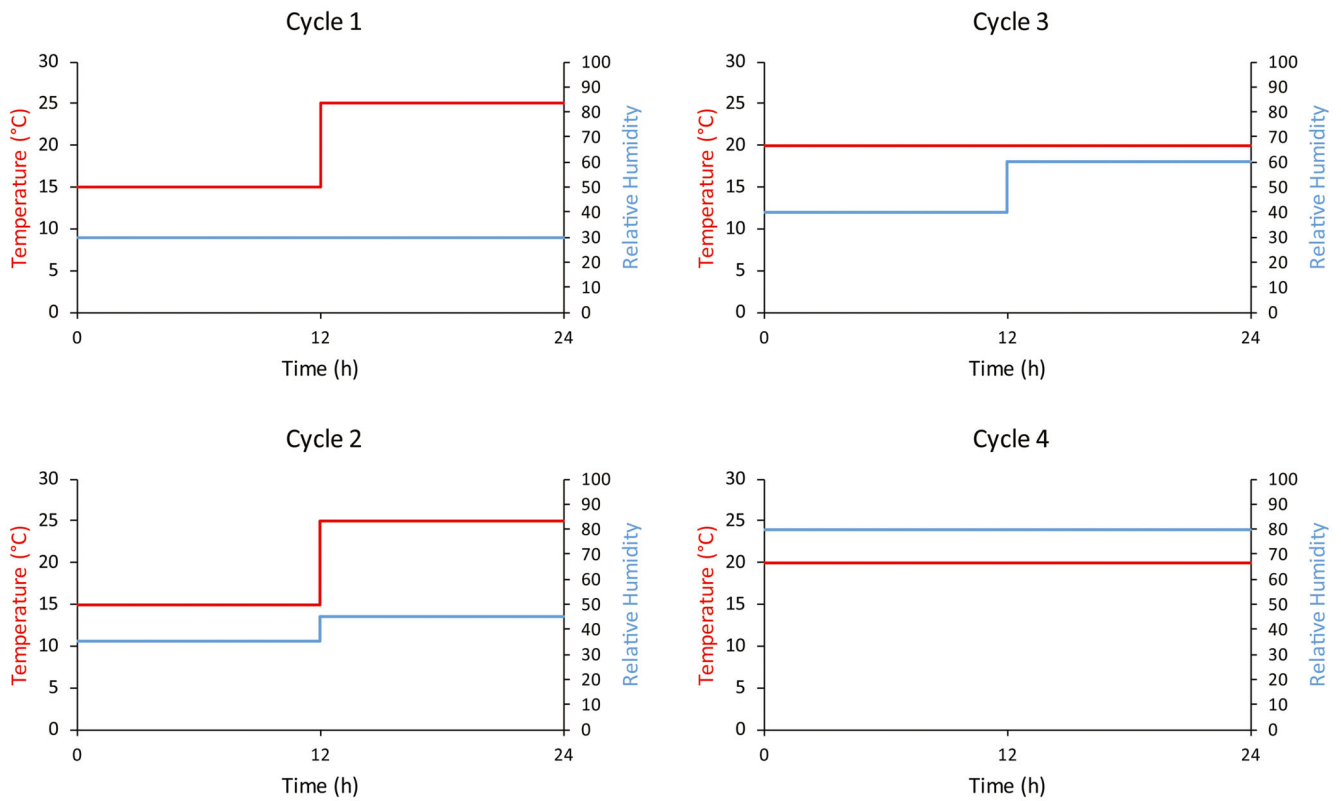

Fig. 3. Diagrams showing the daily-based experimental conditions for each of the four weathering cycles, in terms of temperature (°C) and humidity (%). (Color figure can be viewed at wileyonlinelibrary.com.)

chondrites, such as mineral dissolution, efflorescence, and formation of secondary phases such as ferrihydrite (Bland et al., 2006). However, after MET-2 went through the second weathering cycle, weathering products were observed in the drilled cavities exclusively, with limited spreading on the polished surface of the sample (Fig. 4). These weathering products line the walls of the drilled cavities, suggesting that they were produced during the weathering experiment rather than during storage in the Antarctic environment.

After the subsequent weathering cycles, weathering products are partially covering samples MET-3, MET-4, and MET-5 and are identified on optical images as a red-brownish color characteristic of "metallic rust" (Fig. 5a, 5d, and 5g), which typically results from the oxidation of metallic (Fe^0) or ferrous (Fe^{2+}) to ferric (Fe^{3+}) iron. Weathering products appear as overgrowths on the polished surface of the samples. The roughness of these products with respect to the polished surface distinguishes them easily from other phases using reflected light (Fig. 5b, 5e, and 5h).

The extent of weathering by total surface area varies from 1% in MET-4 to 13% in MET-5. It is noteworthy that this extent does not represent the percentage of sample surface that was altered but rather the spread of weathering overgrowths on the polished surfaces of the samples. In both MET-3 and MET-4, the weathering products mainly occur on the border of the sample with epoxy resin, whereas for MET-5, they also occur in the inner parts of the sample.

In some instances, early onset of weathering products is systematically associated with FeNi metal (Fig. 6). The morphology of weathering products does not vary from one weathered area to the other, even when associated with FeNi only, suggesting that this latter phase is the only mineral phase affected by weathering.

Petrography of Weathering Products

Results of the petrographic study of the samples after the weathering experiments are summarized in Table 1.

In all weathered samples, the only observed weathering products are Fe-oxide/oxyhydroxides, which include a range of minerals that cannot be identified using SEM-EDS due to their fine-grained nature (i.e., micrometer to submicrometer size) and their wide range of chemical compositions (e.g., Lee & Bland, 2004). In most cases, weathering products occur as tubular and/or subspherical shells of poorly crystalline material, with sizes ranging from a few tens up to several hundreds of

19455100, 2022, 6, Downloaded from https://onlinelibrary.wiley.com/doi/10.1111/maps.13818 by EVIDENCE AID - BELGIUM, Wiley Online Library on [07/06/2023]. See the Terms and Conditions (https://onlinelibrary.wiley.com/terms-and-conditions) on Wiley Online Library for rules of use; OA articles are governed by the applicable Creative Commons License

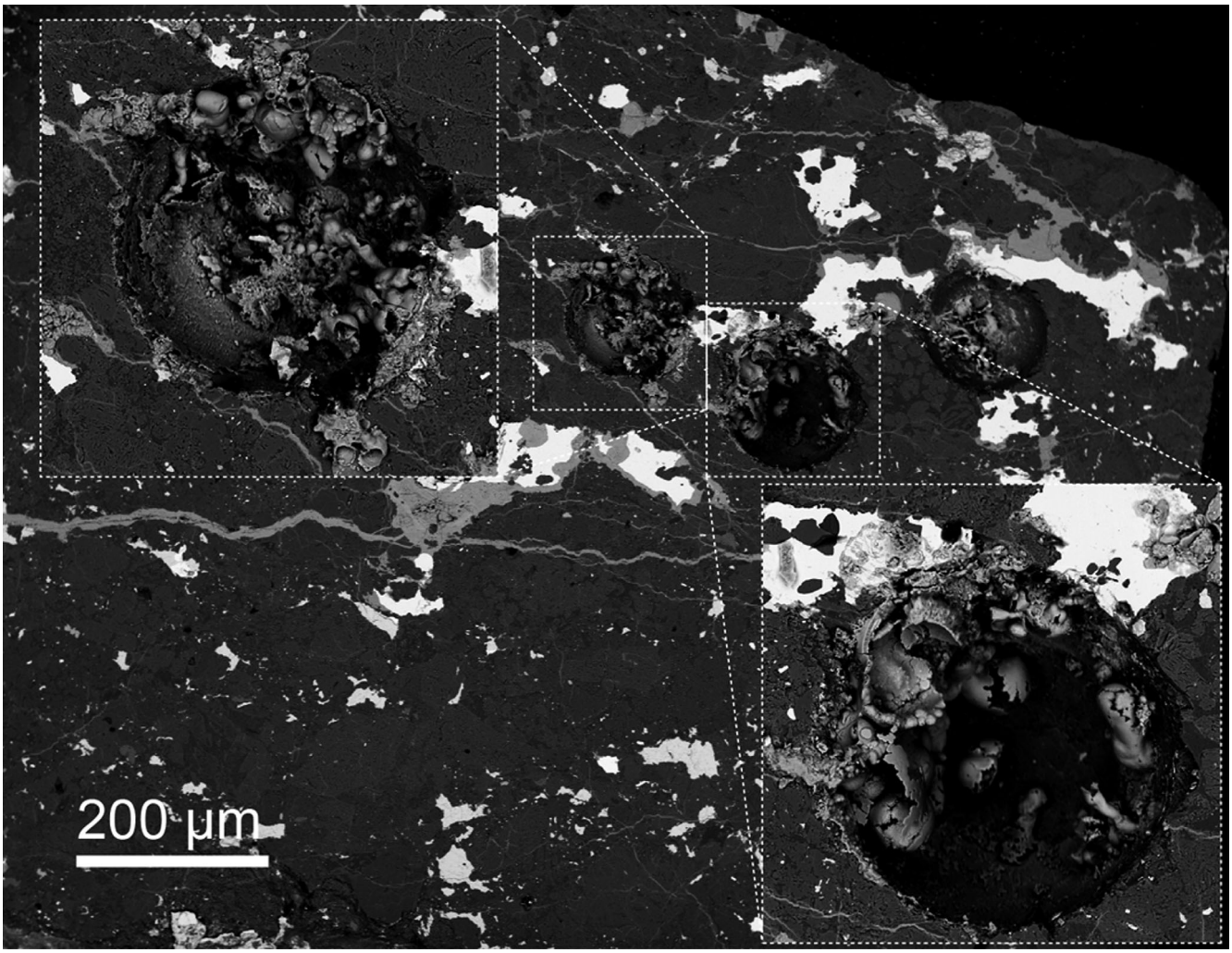

Fig. 4. Scanning electron backscattered image of a drill cavity in MET-2 after the second cycle of weathering. Abundant tubular overgrowths are in the cavity, which consist essentially of iron oxide with Cl detectable with EDS.

micrometers (Fig. 7). The poorly crystalline nature of these weathering products prevents a clear identification using SEM only.

Some occurrences of incomplete shelled structures are observed, exhibiting crystalline material in their interior (Fig. 8). These iron oxide/oxyhydroxide structures are consistent with FeOOH materials, such as akaganeite, lepidocrocite, or goethite, which are commonly associated with the aqueous alteration of metallic iron in a humid environment (e.g., Selwyn et al., 1999). The innermost part of these structures exhibits "cigar-shaped" crystals resembling akaganeite (Fig. 8a), whereas in some instances, the broken side of the walls of the structures appears to have evolved to a more globular morphology (Fig. 8b). Other areas exhibit "cotton-ball" crystals typical of akaganeite above an area of "fine plate" crystals typical of lepidocrocite (Fig. 8c). "Cotton-ball" crystals typical of akaganeite are often observed as well (Fig. 8d).

Chemical Composition of Weathering Phases

Energy-dispersive spectroscopy analyses of weathering phases in MET-3 and MET-5 are shown in Table 2. Corresponding areas of analyses and EDS spectra are shown in Fig. A3 in supporting information. In all occurrences, the weathering products consist of Fe-rich material (>49.2 wt%), with a significant amount of Ni ranging from 1.63 to 13.3 wt%. Minor concentrations of Mg and Si are observed in most analyses of MET-3 and in about half analyses of MET-5, ranging from 0.14 to 2.78 wt % and 0.154 to 0.48 wt%, respectively. Most weathering phases observed in MET-5 contain minor amounts of Cl, ranging from 0.10 to 1.81 wt%. Sulfur is present in weathering products of MET-3 (0.16–0.29 wt%) but below detection limit in weathering products of MET-5.

19455100, 2022, 6, Downloaded from https://onlinelibrary.wiley.com/doi/10.1111/maps.13818 by EVIDENCE AID - BELGIUM, Wiley Online Library on [07/06/2023]. See the Terms and Conditions (https://onlinelibrary.wiley.com/terms-and-conditions) on Wiley Online Library for rules of use; OA articles are governed by the applicable Creative Commons License

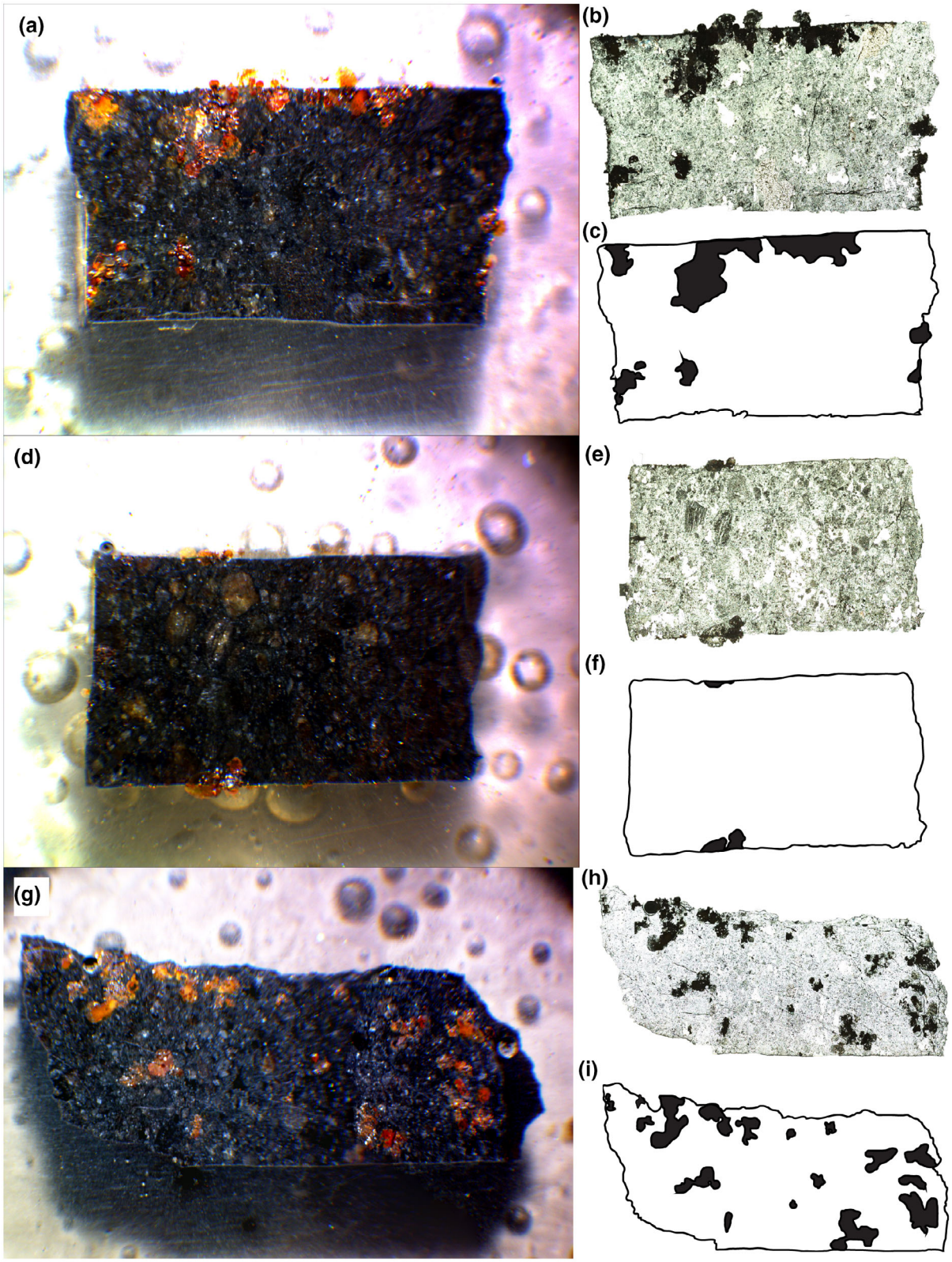

Fig. 5. Extent of weathering after cycles 2, 3, and 4 on MET-3 (a–c), MET-4 (d–f), and MET-5 (g–i), respectively. a, d, g) Weathering products appear as red-brownish, typical of rust, on optical images of the samples. b, e, h) Reflected light image of the samples, on which the weathering products appear black compared to the light, very reflective background. c, f, i) Vector image showing the spread of weathering products (i.e., black areas). (Color figure can be viewed at wileyonlinelibrary.com.)

19455100, 2022, 6, Downloaded from https://onlinelibrary.wiley.com/doi/10.1111/maps.13818 by EVIDENCE AID - BELGIUM, Wiley Online Library on [07/06/2023]. See the Terms and Conditions (https://onlinelibrary.wiley.com/terms-and-conditions) on Wiley Online Library for rules of use; OA articles are governed by the applicable Creative Commons License

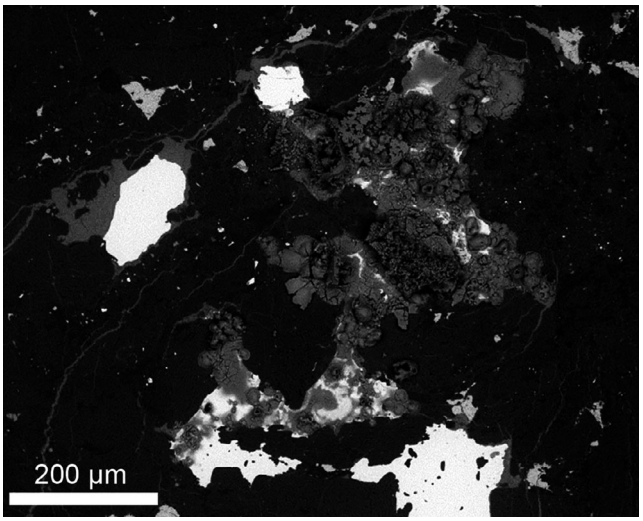

Fig. 6. Scanning electron backscattered image of a weathered area of MET-5 showing that, at an early stage, weathering products are associated with FeNi metal.

Element maps of MET-3, MET-4, and MET-5 show that weathering products are essentially made of Fe (Figs. 9–11). Chlorine is ubiquitous in weathering products, although concentrations vary significantly, with the occurrence of "hot spots" associated with tubular or shelled structures. All weathering products inherited Ni from the FeNi metal to various extents, showing that they are mostly derived from this mineral phase.

Mössbauer Spectroscopy

Drilled powder of samples MET-1 and MET-2 containing weathering material was analyzed using Mössbauer spectroscopy. This technique is extensively used to study the alteration of meteorites as it allows determining the degree of ferric oxidation of primary iron-bearing phases resulting for terrestrial weathering (Bland et al., 1998, 2006; Munayco et al., 2013, 2014). The aim of these analyses was to determine whether the relative amounts of Fe^0, Fe^{2+}, and Fe^{3+} in MET-2 were different from the control sample, MET-1. The Mössbauer spectra of MET-1 and MET-2 after the second cycle of weathering are shown in Figs. A5 and A6 in supporting information, respectively. The Mössbauer hyperfine parameters of the doublets, such as isomer shift (IS) and quadrupole splitting (QS), are presented in Table 3.

In both MET-1 and MET-2 powders, five different phases are observed, two of which are magnetic and comprise sextets (red and green in Figs. A5 and A6). The red sextet corresponds to the hyperfine parameters of the FeNi metal phase kamacite. The green sextet appears to correspond to a sulfide, likely troilite (FeS). The subspectra from the remaining phases are simple doublets. The blue doublet is consistent with olivine, whereas the lavender one is likely related to pyroxene. The brown doublet (2) has hyperfine parameters corresponding to Fe oxyhydroxide. As mentioned previously, A10177 has suffered terrestrial weathering to a certain extent before being collected on the Antarctic ice, as evidenced by the weathering rinds around FeNi metal grains and veins of Fe oxyhydroxide. It appears that weathering products obtained during the experiments are indistinguishable from the ferrihydrite resulting from terrestrial weathering. The relative abundance of the phases observed is identical in both Mössbauer spectra, suggesting that the minute amount of weathering products resulting from the weathering experiment of MET-2 is not readily identified using this technique.

Table 1. Petrographic characteristics of samples after respective weathering experiments. Experimental conditions for each cycle are illustrated in Fig. 3.

Sample	Weathering cycles	Petrography of FeNi metal and troilite	Evidence of silicate dissolution	% surface extension of alteration	Secondary phases	Comment
MET-1	Witness sample	No alteration	No	N/A	None	
MET-2	1	Limited alteration of FeNi grains	No	<1	Tubular Cl-bearing Fe oxyhydroxide	In drilled cavities only
MET-3	2	Limited alteration of FeNi grains	No	12	Tubular + fibrillar Cl-bearing Fe oxyhydroxide	Border of the sample
MET-4	3	Partial alteration of FeNi grains	No	1	Tubular + fibrillar Cl-bearing Fe oxyhydroxide	Border of the sample
MET-5	4	Partial alteration FeNi grains + troilite	No	13	Tubular + fibrillar Cl-bearing Fe oxyhydroxide	

19455100, 2022, 6, Downloaded from https://onlinelibrary.wiley.com/doi/10.1111/maps.13818 by EVIDENCE AID - BELGIUM, Wiley Online Library on [07/06/2023]. See the Terms and Conditions (https://onlinelibrary.wiley.com/terms-and-conditions) on Wiley Online Library for rules of use; OA articles are governed by the applicable Creative Commons License

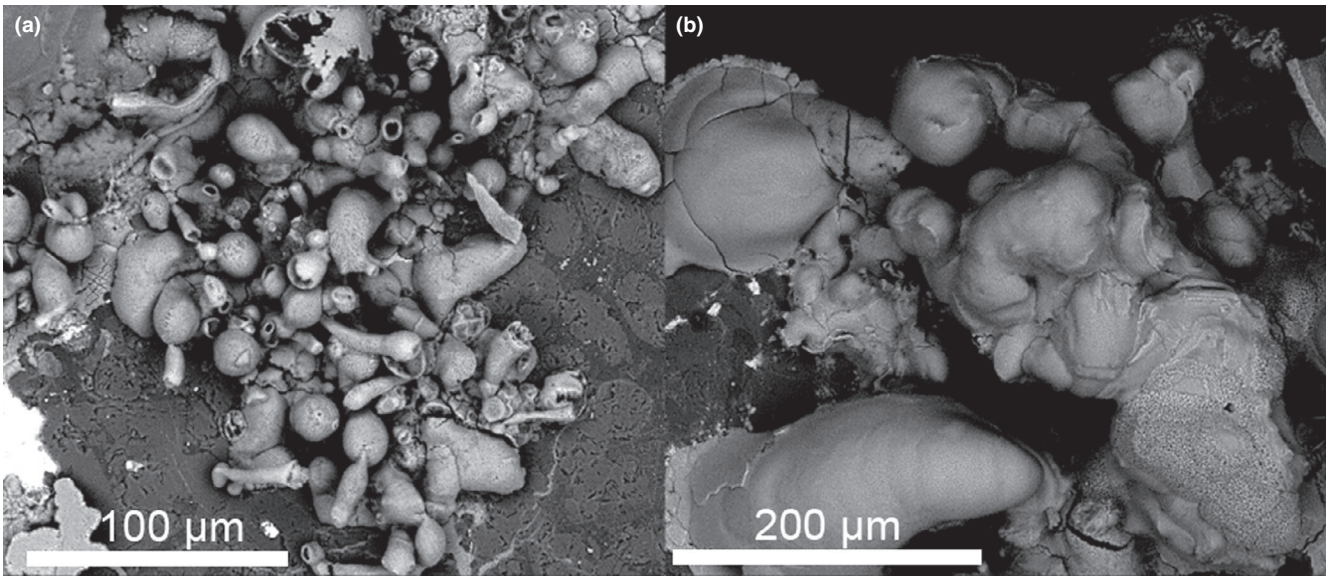

Fig. 7. Scanning electron backscattered image of tubular weathering products on the surface of (a) MET-3 and (b) MET-4.

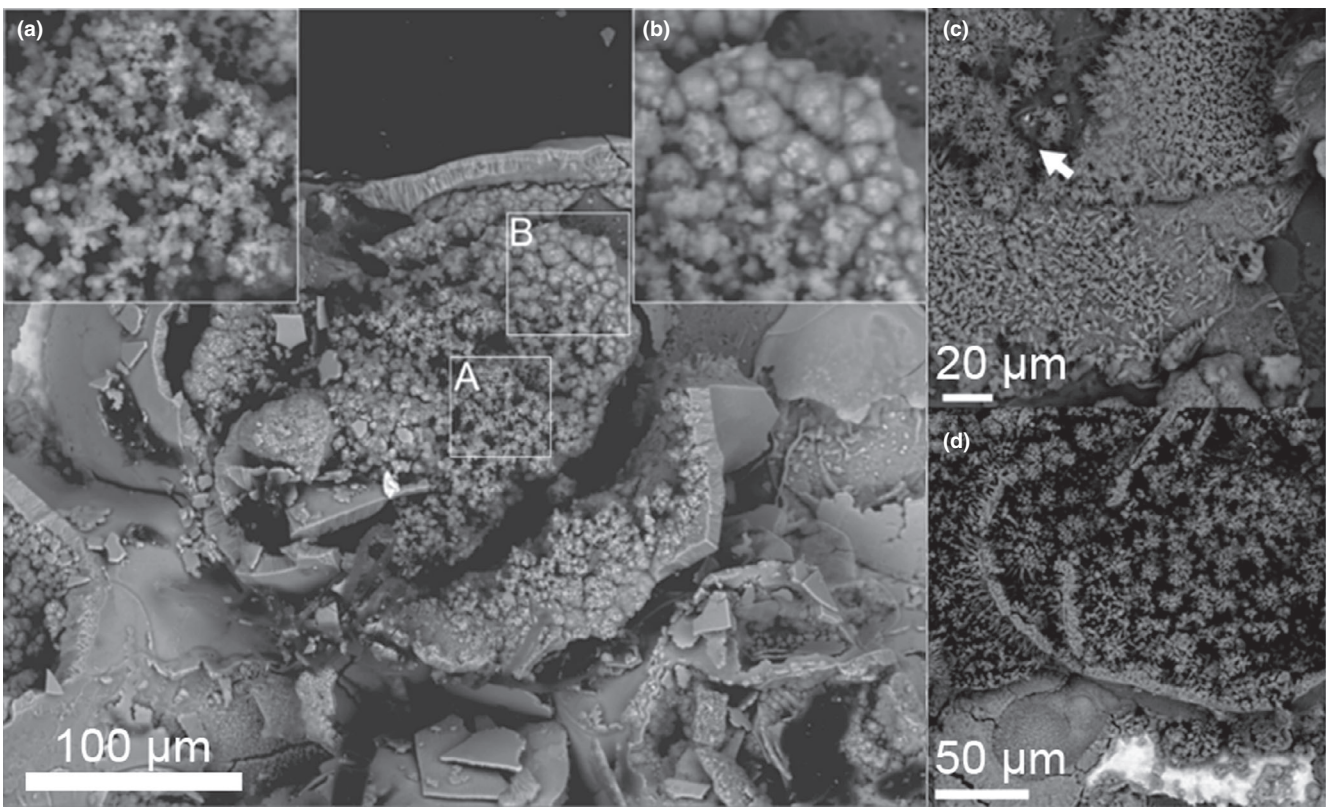

Fig. 8. Scanning electron backscattered image of a "collapsed" shelled structure on MET-3 and MET-5. a) The material in the inner part of the structure shows "cigar-shaped" crystals, typical of akaganeite. b) "Globular" structures typical of goethite. c) Arrowed are "cotton-ball" crystals typical of akaganeite above an area of "fine plates" crystals typical of lepidocrocite. d) The interior of some shelled structures is exclusively comprised of "cotton-ball" crystals typical of akaganeite.

Raman Spectroscopy

The Raman spectra obtained on MET-3, MET-4, and MET-5 are shown in Figs. 12–14, respectively. The collected spectra were compared to minerals in the RRUFF online database and show that a significant part of weathering products exhibits Raman peaks at approximately 250, 295, 380, and 525 cm^{-1}, which

19455100, 2022, 6, Downloaded from https://onlinelibrary.wiley.com/doi/10.1111/maps.13818 by EVIDENCE AID - BELGIUM, Wiley Online Library on [07/06/2023]. See the Terms and Conditions (https://onlinelibrary.wiley.com/terms-and-conditions) on Wiley Online Library for rules of use; OA articles are governed by the applicable Creative Commons License

Table 2. Representative energy-dispersive spectroscopy (EDS) analyses of weathering phases in MET-3 and MET-5. Results in wt% normalized to 100%.

Spectrum	Phase	O	Mg	Si	S	Cl	Fe	Ni
Fig. A3A								
168	Weathering	44.4	0.31	–	0.16	–	49.2	5.79
169	Weathering	29.6	0.41	0.15	0.20	–	67.5	2.01
171	Weathering	45.7	0.23	–	0.20	–	49.9	3.96
172	Weathering	35.3	0.11	–	0.29	–	59.3	4.85
173	Weathering	32.8	2.04	0.48	0.16	–	62.8	1.61
174	Weathering	38.0	2.78	0.27	0.26	–	51.9	6.70
Fig. A3B								
176	FeNi metal	0.0	0.14	0.72	0.08	0.13	79.1	19.8
178	Weathering	33.5	1.34	0.54	–	0.13	55.3	9.24
179	Weathering	25.6	–	0.27	–	0.10	61.5	12.4
Fig. A3C								
180	Weathering	29.2	–	–	–	1.21	57.5	12.1
181	Weathering	29.2	–	–	–	1.81	57.1	11.7
182	Weathering	23.0	–	0.23	–	0.17	63.3	13.3
183	Weathering	22.9	–	0.31	–	0.10	67.3	9.3
184	Weathering	31.5	–	0.24	–	0.14	54.9	13.2
Fig. A3D								
186	Weathering	30.6	–	–	–	1.38	57.8	10.1
187	Weathering	32.8	–	0.17	–	0.19	51.9	15.0

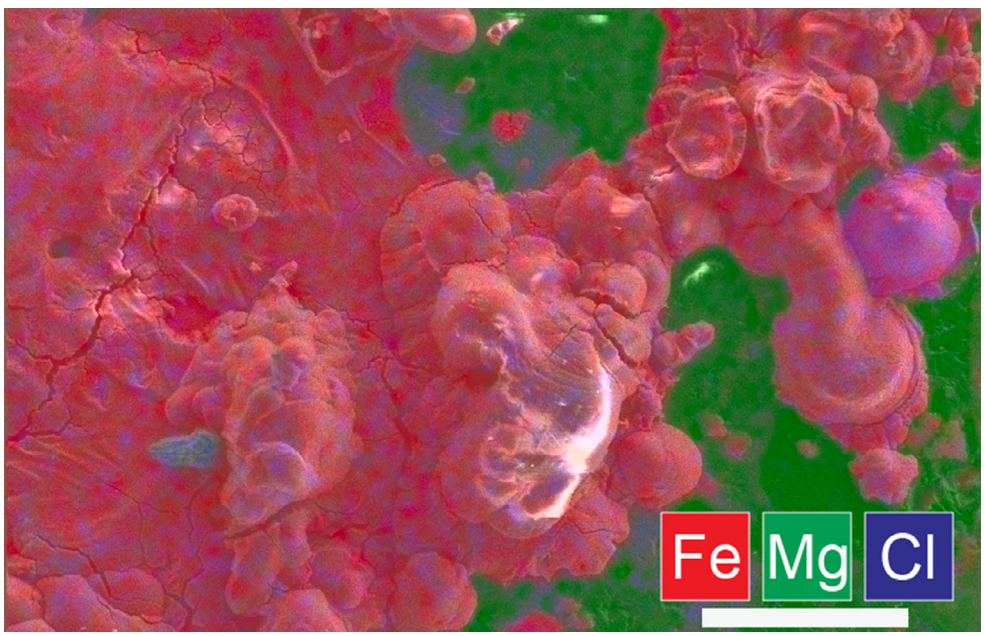

Fig. 9. Major element map of weathering products of MET-3. Chlorine is detected in all products, but only rare "hot spots" are observed. Weathering products are essentially composed of iron oxide. Green and red areas correspond to silicate phases and FeNi metal, respectively. Scale bar is 50 μm. (Color figure can be viewed at wileyonlinelibrary.com.)

match the peaks of lepidocrocite (γ-$Fe^{3+}OOH$) (Figs. 12a, 12b, 14a, and 14c). Another weathering product observed in all samples exhibits peaks at approximately 245, 300, 387, and 549 cm^{-1}, which correspond to goethite (α-$Fe^{3+}OOH$) (Figs. 12c, 13, and 14).

DISCUSSION

^{57}Fe Mössbauer Spectroscopic Analysis

The Mössbauer spectroscopy technique is widely used to determine the valence state of iron in

19455100, 2022, 6, Downloaded from https://onlinelibrary.wiley.com/doi/10.1111/maps.13818 by EVIDENCE AID - BELGIUM, Wiley Online Library on [07/06/2023]. See the Terms and Conditions (https://onlinelibrary.wiley.com/terms-and-conditions) on Wiley Online Library for rules of use; OA articles are governed by the applicable Creative Commons License

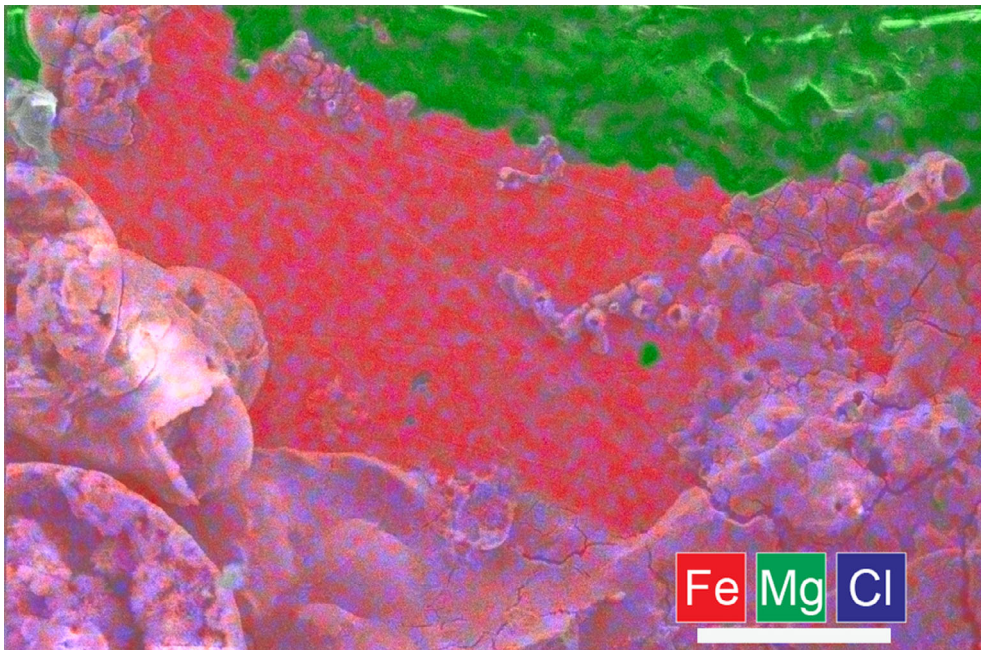

Fig. 10. Major element map of weathering products of MET-4. Chlorine is virtually absent from weathering products in this sample. Weathering products are essentially composed of iron oxide. Green and red areas correspond to silicate phases and FeNi metal, respectively. Scale bar is 30 μm. (Color figure can be viewed at wileyonlinelibrary.com.)

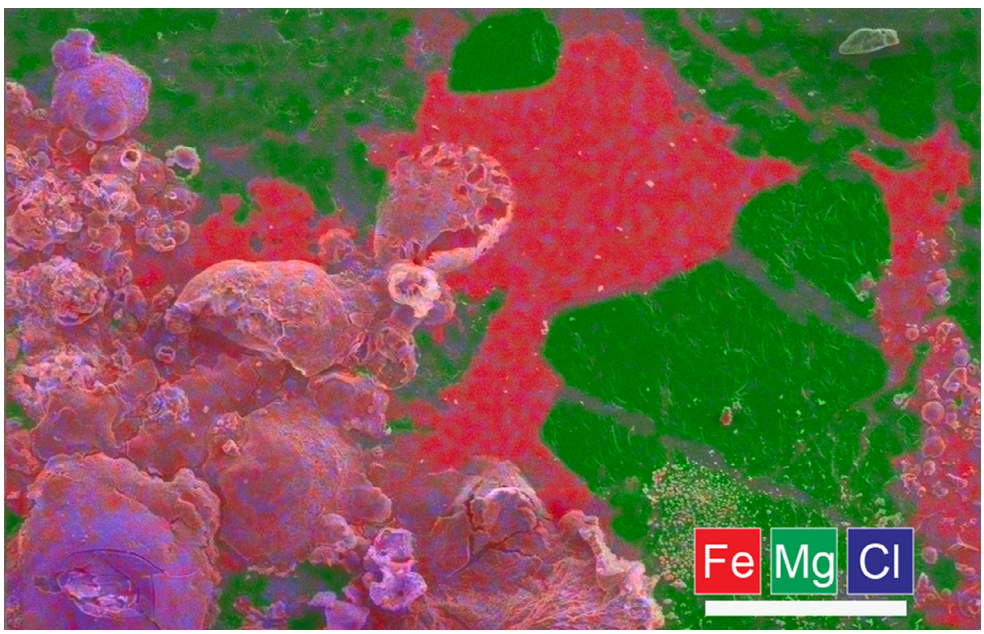

Fig. 11. Major element map of weathering products of MET-5. Tubular structures are usually richer in Cl than surrounding phases. Weathering products are essentially composed of iron oxide. Green and red areas correspond to silicate phases and FeNi metal, respectively. Scale bar is 80 μm. (Color figure can be viewed at wileyonlinelibrary.com.)

geomaterials. In the field of meteoritics, this technique has been extensively used to study the extent of terrestrial weathering by identifying the products of alteration containing ferric iron (Bland et al., 1997, 1998, 2006; Munayco et al., 2013, 2014). Ordinary chondrites that have been collected shortly after their fall, such as Allegan (H5) and Barwell (L6), mainly contain metallic iron (Fe^0; FeNi metal, troilite) and

19455100, 2022, 6, Downloaded from https://onlinelibrary.wiley.com/doi/10.1111/maps.13818 by EVIDENCE AID - BELGIUM, Wiley Online Library on [07/06/2023]. See the Terms and Conditions (https://onlinelibrary.wiley.com/terms-and-conditions) on Wiley Online Library for rules of use; OA articles are governed by the applicable Creative Commons License

Table 3. Mössbauer parameters of the phases constituting MET-1 and MET-2 powders. IS, QS, and Bhf are the isomer shift, quadrupole splitting, and hyperfine magnetic field, respectively.

	MET-1			MET-2		
	IS (mm s^{-1})	QS (mm s^{-1})	Bhf (T)	IS (mm s^{-1})	QS (mm s^{-1})	Bhf (T)
Sextet 1	0.01	0.00	33.9	0.01	0.01	33.8
Sextet 2	0.64	−0.42	30.0	0.59	−0.24	29.7
Doublet 1	1.16	2.97	N/A	1.15	2.95	N/A
Doublet 2	0.45	0.73	N/A	0.44	0.71	N/A
Doublet 3	1.07	2.28	N/A	1.04	2.30	N/A

divalent iron (Fe^{2+}; silicates), and virtually no trivalent iron (Fe^{3+}) resulting from oxidation of these primary mineral phases. Studies using Mössbauer technique have shown that the degree of oxidation increases with increasing terrestrial age (i.e., time since the fall), while the relative abundance of the primary phase decreases (Bland et al., 2006). These observations are consistent with results from studies of bulk magnetic properties or saturation magnetization of meteorites (Rochette et al., 2012; Uehara et al., 2012). This increase in oxidation with time occurs regardless of the environment in which the chondrites were collected, with Antarctic meteorites several tens of thousands of years old exhibiting up to 80% total oxidation. Indeed, even if the climatic conditions in Antarctica are ideal to preserve meteorites from terrestrial weathering (i.e., dry and cold), under certain extreme conditions, liquid water may appear as a monoatomic layer on minerals or even filling pores. This is mainly because their dark color means they absorb sunlight resulting in sporadic heating of the meteorites up to temperatures above the freezing point of water during austral summer. Interaction with water efficiently oxidizes Fe^0 and Fe^{2+} to Fe^{3+}, resulting in the formation of Fe oxyhydroxides, which include magnetite, maghemite (γ-Fe_2O_3), ferrihydrite, lepidocrocite (γ-FeOOH), goethite (α-FeOOH), and akaganeite (β-FeOOH). It is noteworthy that all Fe-bearing phases are affected by oxidation and contribute to the formation of these weathering products. However, FeNi metal is the mineral phase that is most susceptible to weathering, before sulfides and, finally, silicates. In the case of A10177, blank sample MET-1 has been maintained under controlled climatic conditions since its recovery in Antarctica, limiting terrestrial alteration. However, the presence of Fe oxyhydroxide resulting from terrestrial weathering in the field prior to the recovery is obvious around most FeNi metal grains and filling veins (Fig. 2). Figure A5 shows that the Mössbauer spectrum of powder from MET-1 includes a doublet characteristic of Fe^{3+}-bearing oxyhydroxide. Table 3 shows hyperfine parameters IS and QS matching those of "mature" weathering products observed in Antarctic chondrites (Bland et al., 1998). It is not clear whether this material corresponds to goethite or lepidocrocite, but it appears clear that akaganeite, which is usually the first corrosion product of FeNi metal in chondrites, is absent. This absence is expected as lepidocrocite and goethite are common aging products of akaganeite in Antarctic chondrites (e.g., Bland et al., 2006). As observed in Fig. 4, weathering products formed as a result of weathering cycle 2. Their structure and chemistry suggest that these are Fe oxyhydroxides. Thus, the relative abundance of Fe^{3+} is expected to be higher in MET-2 compared to MET-1, considering that the experiments oxidized FeNi metal to form metallic rust. However, the relative amount of the Fe^{3+}-bearing oxyhydroxides is identical in both MET-1 and MET-2. A likely explanation is that the signal from weathering products that was present prior to the experiment obscures the contribution of weathering products resulting from the experiments. Indeed, to run one analysis, at least 1 mg of powder is necessary, requiring drilling out a significant quantity of material. This difficulty in identifying newly formed weathering products using Mössbauer spectroscopy prevented the analyses of more samples (i.e., MET-3, MET-4, and MET-5) to avoid drilling them needlessly. The destructive nature of this technique in the present case further encouraged the use of nondestructive Raman spectroscopy for the later samples, a technique that is readily available and requires virtually no sample preparation.

The Weathering of A10177 Under Laboratory Conditions

Identifying weathering products resulting from the weathering experiments is critical to understand how alteration proceeds in ordinary chondrites under various climatic conditions. Previous studies have shown that terrestrial weathering results in a precise set of products that are common to certain types of climatic conditions, chondrite types, and availability of reactive solutions (Benoit & Sears, 1999; Bland et al., 2006; Gooding, 1982, 1986; Jull et al., 1988; Lee & Bland, 2004;

19455100, 2022, 6, Downloaded from https://onlinelibrary.wiley.com/doi/10.1111/maps.13818 by EVIDENCE AID - BELGIUM, Wiley Online Library on [07/06/2023]. See the Terms and Conditions (https://onlinelibrary.wiley.com/terms-and-conditions) on Wiley Online Library for rules of use; OA articles are governed by the applicable Creative Commons License

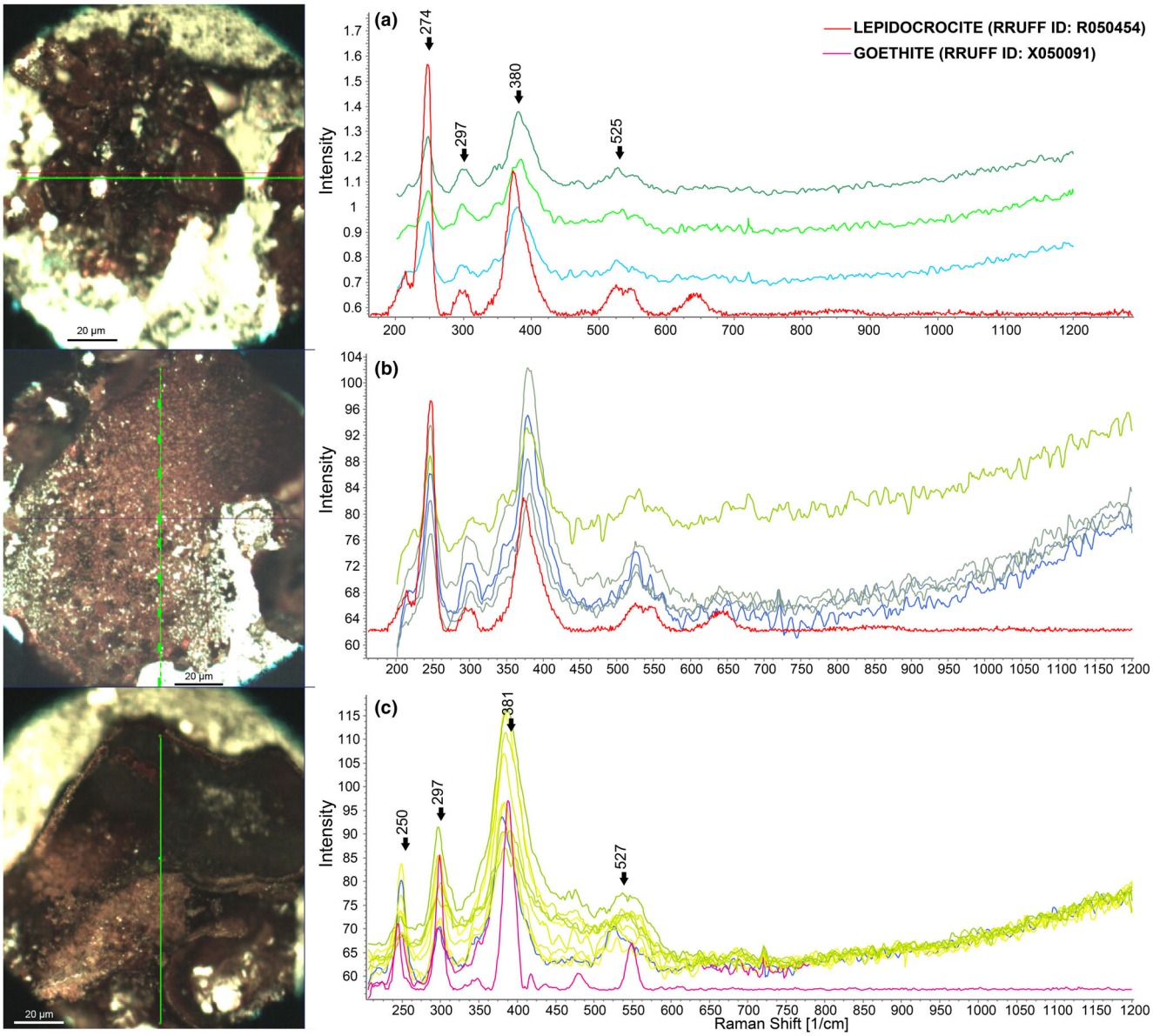

Fig. 12. Raman spectra of weathering products in MET-3. All line analyses (green lines on optical images). a, b) Most weathering products show a match with the spectrum of lepidocrocite (red line; RRUFF ID: R050554). c) Some weathering products show a match with goethite (magenta line; RRUFF ID: X050091). (Color figure can be viewed at wileyonlinelibrary.com.)

Losiak & Velbel, 2011; Velbel, 1988, 2014; Velbel & Gooding, 1990). Furthermore, minerals constituting ordinary chondrites show variable weathering susceptibilities and rates. When water is the main solvent interacting with chondrites, such as in the present study, the sequence of alteration is rather simple and is as follows: FeNi metal > troilite > mafic silicates. The nature of the weathering products depends mainly on the elements released in the solution. The high susceptibility to weathering of FeNi metal with respect to other mineral phases results in ferruginous oxidation minerals as the most commonly observed weathering products. Gooding (1986) recognized two types of corrosion products in ordinary chondrites: "metallic" rust and the "sialic" rust. Metallic rust essentially results from the weathering of metallic iron-bearing phases, such as FeNi metal and troilite, whereas sialic (Fe-Si-Al) rust results from the alteration of mafic silicates. Following the sequence of alteration mentioned above, metallic rust is predominant during the first stage of alteration, whereas sialic rust becomes predominant at a later stage, when most if not all FeNi

19455100, 2022, 6, Downloaded from https://onlinelibrary.wiley.com/doi/10.1111/maps.13818 by EVIDENCE AID - BELGIUM, Wiley Online Library on [07/06/2023]. See the Terms and Conditions (https://onlinelibrary.wiley.com/terms-and-conditions) on Wiley Online Library for rules of use; OA articles are governed by the applicable Creative Commons License

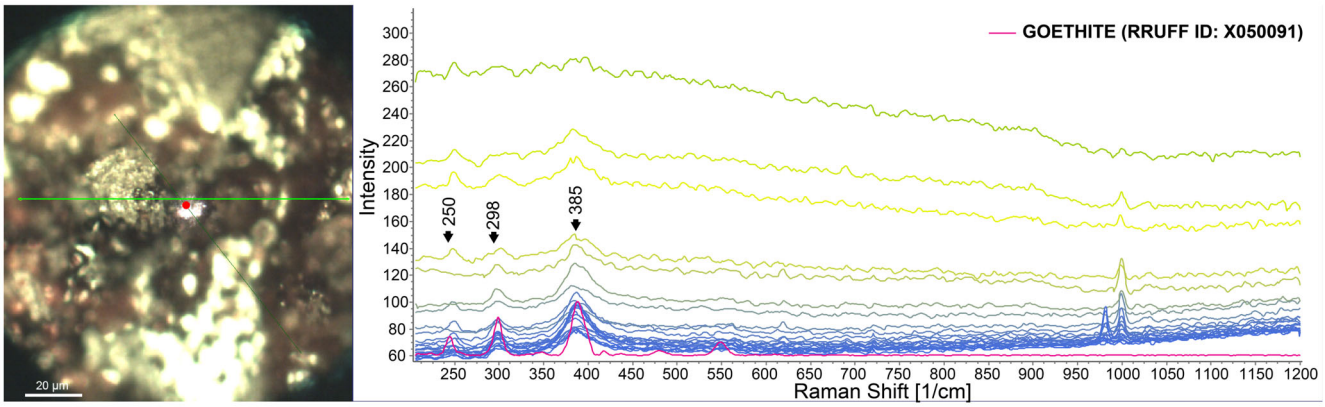

Fig. 13. Raman spectra of weathering products in MET-4. Line analyses (green on optical image) showing good matches with goethite (magenta line; RRUFF ID: X050091). (Color figure can be viewed at wileyonlinelibrary.com.)

metal and troilite are lost and Fe^{2+} in mafic silicates is the main driver of ferruginous oxidation. Identified phases constituting metallic rust in ordinary chondrites include akaganeite (β-FeOOH), goethite (α-FeOOH), lepidocrocite (γ-FeOOH), and maghemite (γ-Fe_2O_3; Buchwald & Clarke, 1989). Several studies have shown that regardless of the climate under which alteration takes place, akaganeite is a key mineral phase resulting from the corrosion of FeNi metal (Bland et al., 1997; Buchwald & Clarke, 1989). The formation of akaganeite involves anodic metal going into solution and being replaced by Cl^- to maintain charge balance (Buchwald & Clarke, 1989). As weathering proceeds, akaganeite can decompose into goethite and/or lepidocrocite, releasing Cl^- ions that will further corrode Fe metal. For this reason, akaganeite is commonly found at the interface with FeNi metal in areas exhibiting early-stage weathering, whereas late-stage weathering areas more likely exhibit intergrowths of lepidocrocite and goethite. Identifying this set of minerals in the examined samples allows reconstruction of their weathering history.

Raman spectroscopy best identifies the weathering products resulting from the experiments. This technique is preferred for several reasons, including (1) its accessibility (e.g., at the RBINS and University of Kent); (2) its ease of use, as it does not require sample preparation; and (3) the analysis of spectral properties of surface material implies that only the weathering outgrowths are examined, which is important as it avoids analyzing Fe oxyhydroxides that predate the experiments. Although this technique is not used to characterize weathering products in meteorites per se, it has been used in several studies as the main tool to investigate corrosion products of iron metal under laboratory and natural conditions (e.g., Cambier et al., 2014; Neff et al., 2004; Oh et al., 1998). With spectra from the RRUFF online database (Lafuente et al., 2016) as references, lepidocrocite and goethite were identified as weathering products in MET-3 and MET-5, while only goethite was observed in MET-4 (Figs. 12–14). Akaganeite is yet to be added to the RRUFF database. Consequently, reference spectra from the literature were used instead (Cambier et al., 2014; Sklute et al., 2018); akaganeite was not identified on the Raman spectra. This may be due to the fact that minor akaganeite content resulted in a minor contribution to the resulting Raman spectra with respect to lepidocrocite and goethite, or simply that akaganeite was not present in the areas analyzed. SEM surveys of weathered areas on the other hand show "cotton-ball" structures and "cigar-shaped" crystals typical of akaganeite, associated with structures and crystal habits typical of lepidocrocite and goethite (Fig. 7). Furthermore, EDS analyses indicate areas with detectable Cl with concentrations up to 1.81 wt%, which is consistent with akaganeite and not lepidocrocite and goethite (Table 2). Element maps also show that high-Cl contents are not ubiquitous in weathering products but are rather limited to "hot spots," probably highlighting newly formed akaganeite (Figs. 9–11). The presence of S in weathering products of MET-3 and in some products on MET-5 suggests that alteration of troilite may have started by the time the weathering cycle ended.

Aside from the weathering of metallic phases, another important aspect of the weathering of chondrites is the dissolution of mafic silicates and subsequent precipitation of weathering products, such as Fe-rich phyllosilicates. In Antarctic meteorites, cronstedtite ($Fe^{2+}{}_2Fe^{3+}[SiFe^{3+}]O_5[OH]_4$) has been observed as a weathering product of ferromagnesian silicates (Lee & Bland, 2004). For example, early-stage alteration of natural and meteoritic olivine is

19455100, 2022, 6, Downloaded from https://onlinelibrary.wiley.com/doi/10.1111/maps.13818 by EVIDENCE AID - BELGIUM, Wiley Online Library on [07/06/2023]. See the Terms and Conditions (https://onlinelibrary.wiley.com/terms-and-conditions) on Wiley Online Library for rules of use; OA articles are governed by the applicable Creative Commons License

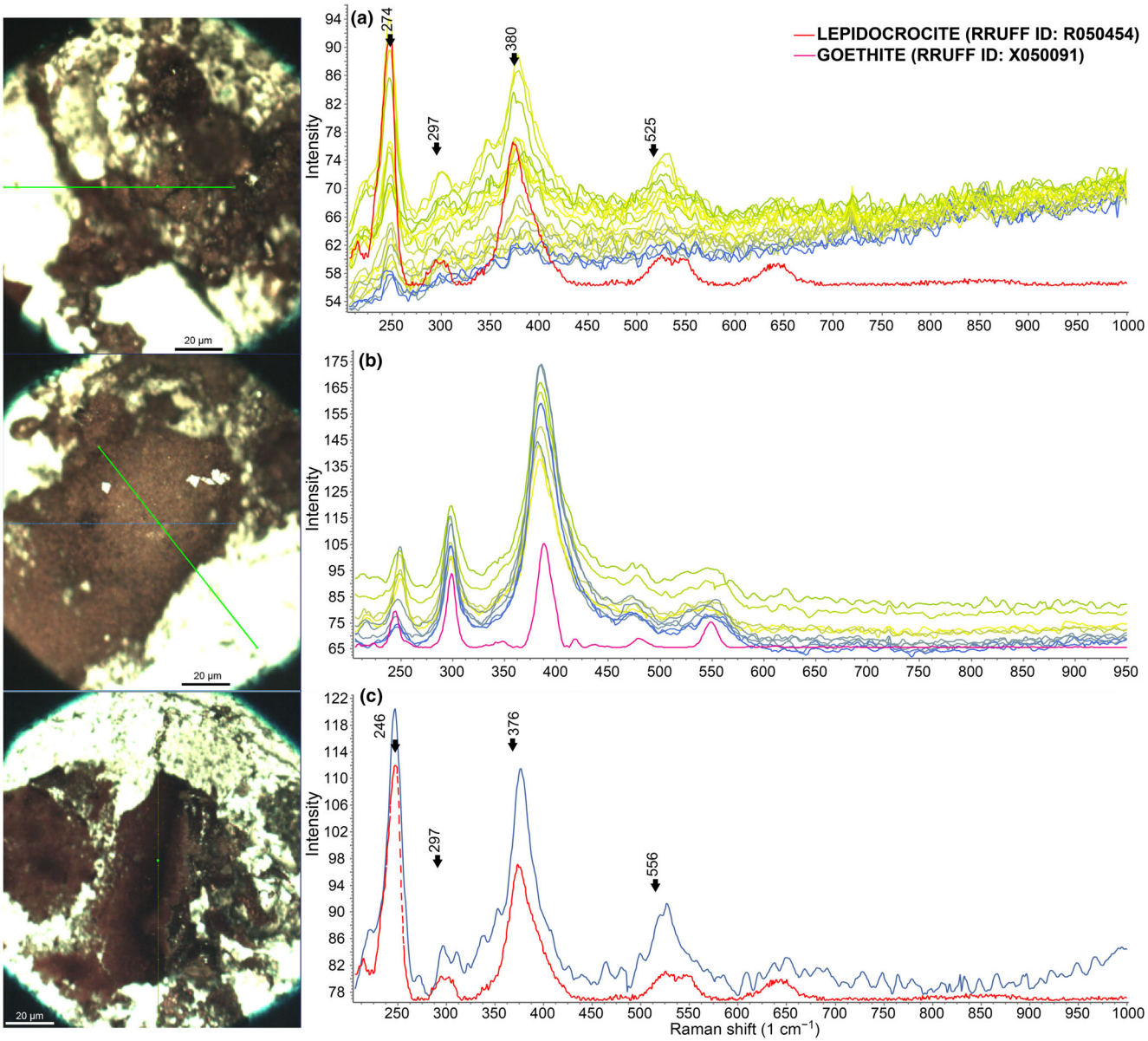

Fig. 14. Raman spectra of weathering products in MET-5. a, b) Line analyses (green lines on optical images) and (c) a point analysis (green point). a, b) Most weathering products show a match with the spectrum of lepidocrocite (red line; RRUFF ID: R050554). c) Some weathering products show a match with goethite (magenta line; RRUFF ID: X050091). (Color figure can be viewed at wileyonlinelibrary.com.)

characterized by the presence of "wedge-shaped" dissolution features along the edge of the crystals (Van Ginneken et al., 2016; Velbel, 2009). Such features are not detected using SEM-EDS on olivine crystals of MET-3, MET-4, and MET-5. Some Si and Mg is detected in EDS analyses of the weathering products of MET-3 and MET-5. However, it is not clear if these result from the alteration of ferromagnesian minerals or rather the inclusion of underlying primary crystals due to a large EDS interaction volume. Structures typical of phyllosilicates are not observed during SEM observations, and Raman spectra of weathered phases do not show peaks typical of phyllosilicates (Lafuente et al., 2016). Therefore, it is assumed that ferromagnesian minerals in the studied samples did not suffer from weathering, or at least to a very limited extent.

It appears that weathering products identified in MET-3, MET-4, and MET-5 exhibit the sequence of aqueous alteration typical of meteoritic FeNi metal only. MET-2 displays similar weathering products, but only after going through the second cycle of alteration,

19455100, 2022, 6, Downloaded from https://onlinelibrary.wiley.com/doi/10.1111/maps.13818 by EVIDENCE AID - BELGIUM, Wiley Online Library on [07/06/2023]. See the Terms and Conditions (https://onlinelibrary.wiley.com/terms-and-conditions) on Wiley Online Library for rules of use; OA articles are governed by the applicable Creative Commons License

along with MET-3. MET-2 does not show signs of weathering after the first cycle that consisted in varying temperatures only. This implies that rapid and large variations in humidity and/or very high humidity (cycle 4) result in a high probability of weathering. The shelled and tubular structures observed with SEM in Fig. 7 are identical to features observed on iron metal that was corroded in the natural environment (e.g., fig. 4 in Selwyn et al., 1999). Such shelled structures occur when droplets of water react with iron metal, dissolving this metal to release Fe^{2+} in the solution. If Cl from the environment is present, the high surface tension of water droplets induces the precipitation of Cl and Fe^{3+} resulting from the oxidation of Fe^{2+} to form akaganeite. Consequently, liquid water in the form of microscale droplets appears to be the main driver of weathering during the experiment rather than a uniform monolayer wetting the whole sample. More importantly, in cases of comparatively low relative humidity, droplet condensation only occurred at the edges of the samples. At 80% relative humidity, droplet condensation also forms in the inner part of the sample.

The chlorine in the weathering solution does not originate from the demineralized water used for the experiments, since it should contain only trace amounts of this ion. Chlorine, which as mentioned above is a major corrosive agent for FeNi metal, may have originated from sea-spray before being incorporated in weathering products that formed in the Antarctic environment prior to the experiment (Langenauer & Krähenbühl, 1993; Shinonaga et al., 1994). Indeed, studies have shown that it is common for Fe-rich products of alteration resulting from the corrosion of FeNi metal to contain Cl content above 1 wt% (Bland et al., 2006; Lee & Bland, 2004). As mentioned above, the relative humidity used during the experiments remained below 100%, meaning that condensation of water on the samples was theoretically not possible. Note that the samples used for the experiments essentially consisted of polished sections and not rough surfaces, which potentially diminishes the potential for water vapor to condense due to the low surface to volume ratio of the exposed surfaces. This is evidenced by the formation of weathering products on the rough surfaces of drilled cavities of MET-2 that allowed the condensation of water vapor during the first cycle of alteration, whereas the polished surface did not show evidence of interaction with liquid water. Furthermore, hygroscopic materials are known to absorb moisture from the air. Primary constituents of ordinary chondrites such as A10177 do not have hygroscopic properties, adding another limiting factor to water condensation under the relative humidity conditions of the experiments. However, Fe oxyhydroxide minerals have hygroscopic properties and are known to present a potential risk of corrosion for metal exposed to the ambient air, even at relative humidity lower than 40% (e.g., Watkinson & Emmerson, 2017; Watkinson & Lewis, 2004; Yeşilbaş & Boily, 2016). Rapid changes in relative humidity are also known to enhance water condensation on Fe oxyhydroxides (Watkinson & Lewis, 2004). Condensation of water droplets on Fe oxyhydroxides resulting from terrestrial weathering in the Antarctic environment and subsequent release of chloride from these minerals seems like a probable mechanism explaining the corrosion of FeNi metal of A10177 during the experiments. Capillary condensation, which represents the ability of submicroscopic cavities to condense moisture at relative humidity below 100%, may have contributed to some extent and may explain the preferential corrosion observed at the interface between the epoxy resin and samples MET-3 and MET-4 (Fig. 5a and 5b). It is noteworthy that submicrometer pores represent the most numerous pore spaces in fresh ordinary chondrite falls. However, most pore spaces are efficiently filled with weathering products in chondrite finds, such as those from Antarctica (Britt & Consolmagno, 2003; Consolmagno & Britt, 1998; Li et al., 2019). It is clear from the SEM observations of A10177 that microscopic pores have long been filled with weathering products, preventing capillary condensation. On the studied samples, it is likely that water droplets originated from condensation on hygroscopic Fe oxyhydroxides mainly, with probable effects of capillary condensation where an imperfect interface between the samples and epoxy resin resulted in submicroscopic cavities. Water enriched in chloride started corroding FeNi metal, which in turn formed a new generation of akaganeite, lepidocrocite, and goethite. The formation of new Fe oxyhydroxide probably promoted further condensation of water, resulting in the tubular structures observed. The high relative humidity during cycle 4 resulted in major contribution of condensation of water on Fe oxyhydroxides already present on MET-5, which may explain why this sample shows evidence of FeNi metal on most of its surface, compared to other samples.

Recommendations for the Preservation of Ordinary Chondrites in Meteorite Collections

From their recovery from the field to their storage in museum or research institute collections, meteorites are carefully maintained under controlled environments to greatly reduce the effects of terrestrial weathering (e.g., Righter et al., 2014). This is particularly the case for Antarctic meteorites, which are usually recovered in the field at subzero temperatures and show low alteration

19455100, 2022, 6, Downloaded from https://onlinelibrary.wiley.com/doi/10.1111/maps.13818 by EVIDENCE AID - BELGIUM, Wiley Online Library on [07/06/2023]. See the Terms and Conditions (https://onlinelibrary.wiley.com/terms-and-conditions) on Wiley Online Library for rules of use; OA articles are governed by the applicable Creative Commons License

states compared to meteorites recovered in hot deserts. The collection and transfer of Antarctic meteorites to the curation facility of RBINS follow a precise protocol, which involves their careful packaging in sealed plastic bags in the field, storage at a temperature of −20 °C during their shipment from Antarctic to the NIPR, and subsequent thawing at room temperature (~22–24 °C) under vacuum to avoid interaction with liquid water (Yamaguchi et al., 2012). After cutting using a wire saw without the use of any liquid, meteorites are then sent to the RBINS, where they are stored at carefully controlled stable temperature and relative humidity (De Ceukelaire et al., 2013). The failure to maintain stable environmental conditions can quickly damage meteorites, such as has been the case for meteorites from the 2003 ANSMET expedition. Indeed, the freezer in which these Antarctic meteorites were stored suffered a power loss for approximately 3 weeks, resulting in the thawing of samples (Satterwhite & Righter, 2006). Of the 530 affected samples, about 1% exhibited visible evaporite growth.

The present study illustrates the importance of maintaining stable environmental conditions for the preservation of ordinary chondrites, especially for the ones containing a large amount of FeNi metal such as the H chondrites. Rapid changes in temperature coupled with comparatively low relative humidity (i.e., cycle 1) do not appear to affect FeNi metal grains at the microscopic scale on a relatively short time scale. However, changing the temperature and relative humidity (i.e., cycle 2) appears to quickly result in the corrosion of metal grains. Humidity variations alone (i.e., cycle 3) result in less FeNi metal corrosion compared to modifying both temperature and humidity at the same time. This shows that temperature fluctuations should not be neglected when associated with changes in relative humidity. Storing chondritic samples in constant conditions of high relative humidity (i.e., cycle 4) results in severe corrosion on most of the samples, showing that such conditions should be avoided in particular. All in all, this work confirms the overall importance of maintaining stable conditions of temperature and relative humidity. The latter parameter must be kept below 40%. These recommendations are especially important in the scope of future comparison of relatively pristine meteorites (i.e., falls and Antarctic) with samples returned directly from asteroids, such as Itokawa, Ryugu, and Bennu from the Hayabusa I (JAXA), Hayabusa II (JAXA), and OSIRIS-REx (NASA) missions.

CONCLUSION

Four samples of meteorite A10177 were artificially weathered in a climatic chamber over four 100-day cycles that consisted of varying the temperature and/or humidity. The weathering products resulting from the experiments were identified using SEM-EDS and Raman spectroscopy, a technique that proved useful for this purpose. Modifying only temperature did not result in visible changes at the microscale. Changing temperature and humidity together or varying humidity only resulted in the appearance of a set of weathering products typically observed in Antarctic meteorites that interacted with sporadic melt water: akaganeite (β-FeOOH), goethite (α-FeOOH), and lepidocrocite (γ-FeOOH). These experiments suggest that akaganeite typically occurs during the early stage of weathering and is the alteration of meteoritic FeNi. Goethite and lepidocrocite occur at a later stage and result from akaganeite decomposition. Minor concentrations of S in some weathering products suggest that troilite corrosion occurred, albeit to a limited extent within the frame of the controlled experiments. No evidence of alteration of mafic minerals is observed.

The main conclusion of these experiments is that humidity constitutes the most important factor controlling the weathering of A10177, especially constant high humidity (≥80%), which resulted in the highest amount of weathering products observed. It is therefore crucial for meteorite curation facilities to maintain stable and relatively low (≤40%) humidity for all samples, at all times, from their discovery in the field, during transport, and in the laboratory or curation facility. This is especially critical for the most pristine samples that will be compared to samples returned from asteroids.

Acknowledgments—This work was made possible thanks to the Belgian Science Policy (Belspo) AMUNDSEN project, including funding to MVG. VD thanks the FRS-FNRS for support. PC and SG thank the VUB Strategic Research Program. PW and MVG thank STFC. Kevin Righter is acknowledged for editorial assistance. We thank Phillipe Heck and an anonymous reviewer for their constructive comments.

Data Availability Statement—All data needed to evaluate the conclusions in the paper are present in the paper and/or the supporting information. Additional data related to this paper may be requested from the authors.

Editorial Handling—Dr. Kevin Righter

REFERENCES

Al-Kathiri, A., Hofmann, B. A., Jull, A. J. T., and Gnos, E. 2005. Weathering of Meteorites from Oman: Correlation of Chemical and Mineralogical Weathering Proxies with

19455100, 2022, 6, Downloaded from https://onlinelibrary.wiley.com/doi/10.1111/maps.13818 by EVIDENCE AID - BELGIUM, Wiley Online Library on [07/06/2023]. See the Terms and Conditions (https://onlinelibrary.wiley.com/terms-and-conditions) on Wiley Online Library for rules of use; OA articles are governed by the applicable Creative Commons License

^{14}C Terrestrial Ages and the Influence of Soil Chemistry. *Meteoritics & Planetary Science* 40: 1215–39. https://doi.org/10.1111/j.1945-5100.2005.tb00185.x.

Benoit, P. H., and Sears, D. W. G. 1999. Accumulation Mechanisms and the Weathering of Antarctic Equilibrated Ordinary Chondrites. *Journal of Geophysical Research: Planets* 104: 14159–68. https://doi.org/10.1029/1999JE900015.

Bevan, A. W. R. 2006. Desert Meteorites: A History. *Geological Society, London, Special Publications* 256: 325–43. http://sp.lyellcollection.org/content/256/1/325.abstract.

Bland, P. A., Kelley, S. P., Berry, F. J., Cadogan, J. M., and Pillinger, C. T. 1997. Artificial Weathering of the Ordinary Chondrite Allegan; Implications for the Presence of Cl^- as a Structural Component in Akaganeite. *American Mineralogist* 82: 1187–97. https://doi.org/10.2138/am-1997-11-1215.

Bland, P. A., Sexton, A. S., Jull, A. J. T., Bevan, A. W. R., Berry, F. J., Thornley, D. M., Astin, T. R., Britt, D. T., and Pillinger, C. T. 1998. Climate and Rock Weathering: A Study of Terrestrial Age Dated Ordinary Chondritic Meteorites from Hot Desert Regions. *Geochimica et Cosmochimica Acta* 62: 3169–84. http://www.sciencedirect.com/science/article/pii/S0016703798001999.

Bland, P. A., Zolensky, M. E., Benedix, G. K., and Sephton, M. A. 2006. Weathering of Chondritic Meteorites. In *Meteorites and the Early Solar System II*, edited by D. S. Lauretta and H. Y. McSween, 853–67. Tucson, Arizona: University of Arizona Press.

Brandstätter, F. 2006. History of the Meteorite Collection of the Natural History Museum of Vienna. *Geological Society, London, Special Publications* 256: 123–33. https://doi.org/10.1144/gsl.sp.2006.256.01.06.

Brearley, A. J., and Jones, R. H. 1998. Chondritic Meteorites. *Planetary Materials*. https://ci.nii.ac.jp/naid/10020737276/en/.

Britt, D. T., and Consolmagno, G. J. S. J. 2003. Stony Meteorite Porosities and Densities: A Review of the Data Through 2001. *Meteoritics & Planetary Science* 38: 1161–80. https://doi.org/10.1111/j.1945-5100.2003.tb00305.x.

Buchwald, V. F., and Clarke, R. S. 1989. Corrosion of Fe-Ni Alloys by Cl-Containing Akaganeite (β-FeOOH); the Antarctic Meteorite Case. *American Mineralogist* 74: 656–67.

Caillet Komorowski, C. L. V. 2006. The Meteorite Collection of the National Museum of Natural History in Paris, France. *Geological Society, London, Special Publications* 256: 163–204. http://sp.lyellcollection.org/content/256/1/163.abstract.

Cambier, S. M., Verreault, D., and Frankel, G. S. 2014. Raman Investigation of Anodic Undermining of Coated Steel During Environmental Exposure. *CORROSION* 70: 1219–29. https://doi.org/10.5006/1358.

Consolmagno, S. J. G. J., and Britt, D. T. 1998. The Density and Porosity of Meteorites from the Vatican Collection. *Meteoritics & Planetary Science* 33: 1231–41. https://doi.org/10.1111/j.1945-5100.1998.tb01308.x.

de Ceukelaire, M., De Vos, W., and Dusar, M. 2013. A New Curation Facility for Antarctic Meteorites at the Royal Belgian Institute of Natural Sciences, Antarctic Meteorites XXXVI: Papers presented to the Thirty-Sixth Symposium on Antarctic Meteorites. pp. 9–10.

Drouard, A., Gattacceca, J., Hutzler, A., Rochette, P., Braucher, R., Bourlès, D., Gounelle, M. et al. 2019. The Meteorite Flux of the Past 2 m.y. Recorded in the Atacama Desert. *Geology* 47: 673–6. https://doi.org/10.1130/G45831.1.

Ebel, D. S. 2006. History of the American Museum of Natural History Meteorite Collection. *Geological Society, London, Special Publications* 256: 267–89. http://sp.lyellcollection.org/content/256/1/267.abstract.

Fogel, R. 1997. On the Significance of Diopside and Oldhamite in Enstatite Chondrites and Aubrites. *Meteoritics & Planetary Science* 32: 577–91. https://doi.org/10.1111/j.1945-5100.1997.tb01302.x.

Gattacceca, J., Suavet, C., Rochette, P., Weiss, B. P., Winklhofer, M., Uehara, M., and Friedrich, J. M. 2014. Metal Phases in Ordinary Chondrites: Magnetic Hysteresis Properties and Implications for Thermal History. *Meteoritics & Planetary Science* 49: 652–76. https://doi.org/10.1111/maps.12268.

Gooding, J. L. 1982. Mineralogical Aspects of Terrestrial Weathering Effects in Chondrites from Allan Hills, Antarctica. Proceedings, 12th Lunar and Planetary Science Conference. pp. 1105–22.

Gooding, J. L. 1986. Weathering of Stony Meteorites in Antarctica. *International Workshop on Antarctic Meteorites*: 48–54.

Gounelle, M. 2006. The Meteorite Fall at L'Aigle and the Biot Report: Exploring the Cradle of Meteoritics. *Geological Society, London, Special Publications* 256: 73–89. https://sp.lyellcollection.org/content/256/1/73.

Jull, A. J. T. 2001. Terrestrial Ages of Meteorites. In *Accretion of Extraterrestrial Matter Throughout Earth's History*, edited by B. Peucker-Ehrenbrink and B. Schmitz, 241–66. Boston, Massachusetts: Springer US. https://doi.org/10.1007/978-1-4419-8694-8_14.

Jull, A. J. T., Cheng, S., Gooding, J. L., and Velbel, M. A. 1988. Rapid Growth of Magnesium-Carbonate Weathering Products in a Stony Meteorite from Antarctica. *Science* 242: 417–9. http://science.sciencemag.org/content/242/4877/417.abstract.

Kaiden, H., Goderis, S., Vinciane, D., Kojima, H., and Claeys, P. 2011. Joint Belgium-Japan Search for Antarctic Meteorites in the 2010–2011 Field Season. *74th Annual Meteoritical Society Meeting*: 5415.

Kojima, H. 2006. The History of Japanese Antarctic Meteorites. *Geological Society, London, Special Publications* 256: 291–303. https://doi.org/10.1144/GSL.SP.2006.256.01.14.

Krot, A. N., Keil, K., Scott, E. R. D., Goodrich, C. A., and Weisberg, M. K. 2007. 1.05—Classification of Meteorites. In *Treatise on Geochemistry*, edited by H. D. Holland and K. K. Turekian, 1–52. Oxford: Pergamon.

Lafuente, B., Downs, R. T., Yang, H., and Stone, N. 2016. The Power of Databases: The RRUFF Project. In *Highlights in Mineralogical Crystallography*, edited by T. Armbruster and R. M. Danisi, 1–29. Berlin: Walter de Gruyter GmbH.

Langenauer, M., and Krähenbühl, U. 1993. Halogen Contamination in Antarctic H5 and H6 Chondrites and Relation to Sites of Recovery. *Earth and Planetary Science Letters* 120: 431–42. https://www.sciencedirect.com/science/article/pii/0012821X93902558.

Lee, M. R., and Bland, P. A. 2004. Mechanisms of Weathering of Meteorites Recovered from Hot and Cold Deserts and the Formation of Phyllosilicates. *Geochimica et Cosmochimica Acta* 68: 893–916. http://www.sciencedirect.com/science/article/pii/S0016703703004861.

19455100, 2022, 6, Downloaded from https://onlinelibrary.wiley.com/doi/10.1111/maps.13818 by EVIDENCE AID - BELGIUM, Wiley Online Library on [07/06/2023]. See the Terms and Conditions (https://onlinelibrary.wiley.com/terms-and-conditions) on Wiley Online Library for rules of use; OA articles are governed by the applicable Creative Commons License

Li, S. J., Wang, S. J., Miao, B. K., Li, Y., Li, X. Y., Zeng, X. J., and Xia, Z. P. 2019. The Density, Porosity, and Pore Morphology of Fall and Find Ordinary Chondrites. *Journal of Geophysical Research: Planets* 124: 2945–69. https://doi.org/10.1029/2019JE005940.

Losiak, A., and Velbel, M. A. 2011. Evaporite Formation During Weathering of Antarctic Meteorites—A Weathering Census Analysis Based on the ANSMET Database. *Meteoritics & Planetary Science* 46: 443–58. https://doi.org/10.1111/j.1945-5100.2010.01166.x.

Maeda, R., Goderis, S., Debaille, V., Pourkhorsandi, H., Hublet, G., and Claeys, P. 2021. The Effects of Antarctic Alteration and Sample Heterogeneity on Sm-Nd and Lu-Hf Systematics in H Chondrites. *Geochimica et Cosmochimica Acta* 305: 106–29. https://www.sciencedirect.com/science/article/pii/S0016703721002763.

Marvin, U. B. 2006. Meteorites in History: An Overview from the Renaissance to the 20th Century. *Geological Society, London, Special Publications* 256: 15–71. https://sp.lyellcollection.org/content/256/1/15.

McCall, G. J. H., Bowden, A. J., and Howarth, R. J. 2006. The History of Meteoritics—Overview. *Geological Society, London, Special Publications* 256: 1–13. https://sp.lyellcollection.org/content/256/1/1.

McCubbin, F. M., Herd, C. D. K., Yada, T., Hutzler, A., Calaway, M. J., Allton, J. H., Corrigan, C. M. et al. 2019. Advanced Curation of Astromaterials for Planetary Science. *Space Science Reviews* 215: 48. https://doi.org/10.1007/s11214-019-0615-9.

Mittlefehldt, D., McCoy, T. J., Goodrich, C. A., and Kracher, A. 1998. Non-Chondritic Meteorites from Asteroidal Bodies. In *Planetary Materials*. Reviews in Mineralogy and Geochemistry, edited by J. J. Papike, 36, 4.1–4.196. Berlin: De Gruyter.

Munayco, P., Munayco, J., de Avillez, R. R., Valenzuela, M., Rochette, P., Gattacceca, J., and Scorzelli, R. B. 2013. Weathering of Ordinary Chondrites from the Atacama Desert, Chile, by Mössbauer Spectroscopy and Synchrotron Radiation X-Ray Diffraction. *Meteoritics & Planetary Science* 48: 457–73. https://doi.org/10.1111/maps.12067.

Munayco, P., Munayco, J., Valenzuela, M., Rochette, P., Gattacceca, J., and Scorzelli, R. B. 2014. ^{57}Fe Mössbauer Spectroscopy Studies of Chondritic Meteorites from the Atacama Desert, Chile: Implications for Weathering Processes. In *LACAME 2012*, edited by C. A. B. Meneses, E. P. Caetano, C. E. R. Torres, C. Pizarro, and L. E. Z. Alfonso, 251–6. Dordrecht, Netherlands: Springer.

Neff, D., Reguer, S., Bellot-Gurlet, L., Dillmann, P., and Bertholon, R. 2004. Structural Characterization of Corrosion Products on Archaeological Iron: An Integrated Analytical Approach to Establish Corrosion Forms. *Journal of Raman Spectroscopy* 35: 739–45. https://doi.org/10.1002/jrs.1130.

Nishiizumi, K., Elmore, D., and Kubik, P. W. 1989. Update on Terrestrial Ages of Antarctic Meteorites. *Earth and Planetary Science Letters* 93: 299–313. http://www.sciencedirect.com/science/article/pii/0012821X89900290.

Oh, S. J., Cook, D. C., and Townsend, H. E. 1998. Characterization of Iron Oxides Commonly Formed As Corrosion Products on Steel. *Hyperfine Interactions* 112: 59–66. https://doi.org/10.1023/A:1011076308501.

Okada, A., Keil, K., and Taylor, G. J. 1981. Unusual Weathering Products of Oldhamite in the Norton County Enstatite Achondrite. *Meteoritics* 16: 141–52. https://doi.org/10.1111/j.1945-5100.1981.tb00539.x.

Pourkhorsandi, H., Debaille, V., Armytage, R. M. G., van Ginneken, M., Rochette, P., and Gattacceca, J. 2021. The Effects of Terrestrial Weathering on Samarium-Neodymium Isotopic Composition of Ordinary Chondrites. *Chemical Geology* 562: 120056. http://www.sciencedirect.com/science/article/pii/S0009254120305957.

Righter, K., Satterwhite, C. E., McBride, K. M., Corrigan, C. M., and Welzenbach, L. C. 2014. Curation and Allocation of Samples in the U.S. Antarctic Meteorite Collection. In *35 Seasons of U.S. Antarctic Meteorites (1976–2010)*, edited by K. Righter, C. M. Corrigan, T. J. McCoy, and R. P. Harvey, 43–63. Washington, D.C.: American Geophysical Union (AGU). https://doi.org/10.1002/9781118798478.ch3.

Rochette, P., Gattacceca, J., and Lewandowski, M. 2012. Magnetic Classification of Meteorites and Application to the SoBtmany Fall. *Meteorites* 2: 67–71.

Russell, S., and Grady, M. M. 2006. A History of the Meteorite Collection at the Natural History Museum, London. *Geological Society, London, Special Publications* 256: 153–62. https://doi.org/10.1144/gsl.sp.2006.256.01.08.

Ruzicka, A., Grossman, J., Bouvier, A., and Agee, C. B. 2017. The Meteoritical Bulletin, No. 103. *Meteoritics & Planetary Science* 52: 1014. https://doi.org/10.1111/maps.12888.

Satterwhite, C. E., and Righter, K. 2006. Antarctic Meteorite Newsletter. *Antarctic Meteorite Newsletter* 29: 2. http://curator.jsc.nasa.gov/antmet/amn/amnfeb06/AMNfeb06.pdf.

Schlüter, J., Schultz, L., Thiedig, F., Al-Mahdi, B. O., and Aghreb, A. E. A. 2002. The Dar al Gani Meteorite Field (Libyan Sahara): Geological Setting, Pairing of Meteorites, and Recovery Density. *Meteoritics & Planetary Science* 37: 1079–93. https://doi.org/10.1111/j.1945-5100.2002.tb00879.x.

Selwyn, L. S., Sirois, P. J., and Argyropoulos, V. 1999. The Corrosion of Excavated Archaeological Iron with Details on Weeping and Akaganéite. *Studies in Conservation* 44: 217–32. http://www.jstor.org/stable/1506652.

Shinonaga, T., Endo, K., Ebihara, M., Heumann, K. G., and Nakahara, H. 1994. Weathering of Antarctic Meteorites Investigated from Contents of Fe^{3+}, Chlorine, and Iodine. *Geochimica et Cosmochimica Acta* 58: 3735–40. https://www.sciencedirect.com/science/article/pii/0016703794901627.

Sklute, E. C., Kashyap, S., Dyar, M. D., Holden, J. F., Tague, T., Wang, P., and Jaret, S. J. 2018. Spectral and Morphological Characteristics of Synthetic Nanophase Iron (oxyhydr)oxides. *Physics and Chemistry of Minerals* 45: 1–26. https://doi.org/10.1007/s00269-017-0897-y.

Uehara, M., Gattacceca, J., Rochette, P., Demory, F., and Valenzuela, E. M. 2012. Magnetic Study of Meteorites Recovered in the Atacama Desert (Chile): Implications for Meteorite Paleomagnetism and the Stability of Hot Desert Surfaces. *Physics of the Earth and Planetary Interiors* 200–201: 113–23. https://www.sciencedirect.com/science/article/pii/S003192011200074X.

Van Ginneken, M., Genge, M. J., Folco, L., and Harvey, R. P. 2016. The Weathering of Micrometeorites from the Transantarctic Mountains. *Geochimica et Cosmochimica Acta* 179: 1–31. http://www.sciencedirect.com/science/article/pii/S0016703716300011.

19455100, 2022, 6, Downloaded from https://onlinelibrary.wiley.com/doi/10.1111/maps.13818 by EVIDENCE AID - BELGIUM, Wiley Online Library on [07/06/2023]. See the Terms and Conditions (https://onlinelibrary.wiley.com/terms-and-conditions) on Wiley Online Library for rules of use; OA articles are governed by the applicable Creative Commons License

Van Schmus, W. R., and Wood, J. A. 1967. A Chemical-Petrologic Classification for the Chondritic Meteorites. *Geochimica et Cosmochimica Acta* 31: 747–65. https://www.sciencedirect.com/science/article/pii/S0016703767800309.

Velbel, M. A. 1988. The Distribution and Significance of Evaporitic Weathering Products on Antarctic Meteorites. *Meteoritics* 23: 151–9. https://doi.org/10.1111/j.1945-5100.1988.tb00910.x.

Velbel, M. A. 2009. Dissolution of Olivine During Natural Weathering. *Geochimica et Cosmochimica Acta* 73: 6098–113. http://www.sciencedirect.com/science/article/pii/S0016703709004797.

Velbel, M. A. 2014. Terrestrial Weathering of Ordinary Chondrites in Nature and Continuing During Laboratory Storage and Processing: Review and Implications for Hayabusa Sample Integrity. *Meteoritics & Planetary Science* 49: 154–71. https://doi.org/10.1111/j.1945-5100.2012.01405.x.

Velbel, M. A., and Gooding, J. L. 1990. Terrestrial Weathering of Antarctic Stony Meteorites – Developments 1985–1989. Workshop on Differences Between Antarctic and Non-Antarctic Meteorites. pp. 94–8.

Watkinson, D. E., and Emmerson, N. J. 2017. The Impact of Aqueous Washing on the Ability of βFeOOH to Corrode Iron. *Environmental Science and Pollution Research International* 24: 2138–49. https://pubmed.ncbi.nlm.nih.gov/27164877.

Watkinson, D., and Lewis, M. R. T. 2004. The Role of βFeOOH in the Corrosion of Archaeological Iron. *MRS Proceedings* 852: 21–32. https://doi.org/10.1557/PROC-852-OO1.6.

Weisberg, M. K., McCoy, T. J., and Krot, A. N. 2006. Systematics and Evaluation of Meteorite Classification. In *Meteorites and the Early Solar System II*, edited by D. S. Lauretta and H. Y. McSween, 19–52. Tuscon, Arizona: University of Arizona Press.

Welten, K. C., Folco, L., Nishiizumi, K., Caffee, M. W., Grimberg, A., Meier, M. M. M., and Kober, F. 2008. Meteoritic and Bedrock Constraints on the Glacial History of Frontier Mountain in Northern Victoria Land, Antarctica. *Earth and Planetary Science Letters* 270: 308–15. https://www.sciencedirect.com/science/article/pii/S0012821X08002161.

Wlotzka, F. 1993. A Weathering Scale for the Ordinary Chondrites. *Meteoritics* 28: 460.

Yada, T., Fujimura, A., Abe, M., Nakamura, T., Noguchi, T., Okazaki, R., Nagao, K. et al. 2014. Hayabusa-Returned Sample Curation in the Planetary Material Sample Curation Facility of JAXA. *Meteoritics & Planetary Science* 49: 135–53. https://doi.org/10.1111/maps.12027.

Yamaguchi, A., Imae, N., Kojima, H., Ozawa, S., and Kimura, M. 2012. Curation of Antarctic Meteorites at the National Institute of Polar Research: Papers Presented to the Thirty-Fifth Symposium on Antarctic Meteorites. pp. 64–5.

Yeşilbaş, M., and Boily, J.-F. 2016. Particle Size Controls on Water Adsorption and Condensation Regimes at Mineral Surfaces. *Scientific Reports* 6: 32136. https://doi.org/10.1038/srep32136.

Zekollari, H., Goderis, S., Debaille, V., van Ginneken, M., Gattacceca, J., Timothy Jull, A. J., Lenaerts, J. T. M., Yamaguchi, A., Huybrechts, P., and Claeys, P. 2019. Unravelling the High-Altitude Nansen Blue Ice Field Meteorite Trap (East Antarctica) and Implications for Regional Palaeo-Conditions. *Geochimica et Cosmochimica Acta* 248: 289–310. http://www.sciencedirect.com/science/article/pii/S0016703718307245.

SUPPORTING INFORMATION

Additional supporting information may be found in the online version of this article.

Fig. A1. Landsat satellite map of the sampling location of A10177 on the Nansen ice field. PEA: Princess Elizabeth Antarctica station.

Fig. A2. "Incomplete" shelled structures on MET-3.

Fig. A3. Secondary electron images of areas of EDS analyses of weathering products in MET-3 (a) and MET-5 (b–d) and corresponding EDS spectra.

Fig. A4. Major element map of a tubular weathering product of MET-5. Such tubular structures are usually richer in Cl than surrounding phases. Scale bar is 10 μm.

Fig. A5. Mössbauer spectrum (black line) of MET-1 powder. Several sextet and doublets are identified. Red sextet is identified as kamacite; green sextet is identified as an iron sulfide (probably troilite); blue and lavender doublets are identified as olivine and pyroxene, respectively; finally, brown doublet is difficult to identify and may be ferrihydrite.

Fig. A6. Mössbauer spectrum (black line) of MET-2 powder. Peaks are identical as those observed in MET-1.

19455100, 2022, 6, Downloaded from https://onlinelibrary.wiley.com/doi/10.1111/maps.13818 by EVIDENCE AID - BELGIUM, Wiley Online Library on [07/06/2023]. See the Terms and Conditions (https://onlinelibrary.wiley.com/terms-and-conditions) on Wiley Online Library for rules of use; OA articles are governed by the applicable Creative Commons License